Journal of Neuroinflammation

RESEARCH

Open Access

Cigarette smoke-induced lung-brain barrier dysfunction drives neurocognitive impairment via inflammatory spill-over

Xiao Yu[1], Hui Xiao[2], Shilong Bao[3], Yiding Dong[3], Zhiyong Dong[1], Jia Zhao[1], Guoqiang Wang[4], Xiaoting Meng[1*] and Fang Wang[4*]

Abstract

Background Although the association between cigarette smoke (CS)-induced chronic obstructive pulmonary disease (COPD) and neurocognitive disorders is recognized, the underlying mechanisms remain unclear. To date, no studies have linked alterations in lung and brain barrier permeability to the "spill-over" of inflammatory factors in CS induced COPD-related neurocognitive disorders (COPD-NCDs).

Methods Using GWAS data, a two-sample Mendelian randomization (MR) analysis was conducted to explore the genetic associations between COPD and neurocognitive disorders (dementia, Alzheimer's disease, etc.). A BALB/c female mouse model with CS exposure (9 cigarettes/day × 24 weeks) was established. Cognitive functions were evaluated using open field tests, novel object recognition tests, and Morris water maze tests. Histopathological changes were observed by HE and Masson staining. Cellular and molecular profiles in brain tissues were analyzed by single-cell RNA sequencing. Levels of inflammatory factors were detected by ELISA. Barrier permeability changes in the lungs and brain were assessed by using Evans Blue staining. Tight junction proteins in lung and brain tissues were measured by immunofluorescence and Western blotting.

Results MR analysis revealed causal associations between COPD and Alzheimer's disease, dementia, depression, anxiety, and Parkinson's disease. CS-exposed mice exhibited COPD phenotypes (emphysema, reduced lung function) and cognitive impairments (memory deficits, anxiety-like behaviors). Activation of microglia/astrocytes and decreased neuronal/synaptic marker expression were observed in the hippocampus. Increased leakage of Evans blue staining in the lungs and brain, along with downregulated expression of tight junction proteins (Occludin, Claudin1, ZO-1), indicated increased blood-brain barrier (BBB) permeability. Elevated levels of inflammatory factors (IL-1β, IL-6, TNF-α) were detected in lung tissues, brain tissues and serum.

Conclusions CS exposure disrupts lung barrier function, leading to the "spill-over" of inflammatory factors to the brain via the lung-brain axis. This increases BBB permeability, triggering neuroinflammation, impairing hippocampal

*Correspondence:
Xiaoting Meng
mengxt@jlu.edu.cn
Fang Wang
wf@jlu.edu.cn

Full list of author information is available at the end of the article

neuronal and synaptic function, and ultimately causing neurocognitive disorders. This study elucidates a novel mechanism of COPD-NCDs, which may provide new targets for the treatment of COPD-NCDs.

Keywords Cigarette smoke (CS), Chronic obstructive pulmonary disease (COPD), COPD-related neurocognitive disorders (COPD-NCDs), Lung-brain axis, Blood-brain barrier (BBB)

Introduction

Chronic Obstructive Pulmonary Disease (COPD) is a progressive respiratory disorder primarily characterized by persistent airflow obstruction due to irreversible alveolar dysfunction (emphysema) and/or small airway fibrosis (chronic bronchitis), manifesting clinically as chronic cough, dyspnea, and sputum production [1–3]. Tobacco smoking (cigarette smoke, CS) accounts for ~ 80% of COPD cases in industrialized nations [4]. Toxic substances produced by CS (such as reactive carbonyls, heavy metals) can easily cross the biological barriers and trigger multi-system inflammatory responses. For example, in the central nervous system (CNS), COPD patients show activation of microglia cells and mitochondrial oxidative stress, thereby disrupting hippocampal neurogenesis and synaptic plasticity [5, 6]. COPD-related neurocognitive disorders (COPD-NCDs) constitute a prevalent but understudied comorbidity, affecting 61% of COPD patients [7] and is independently associated with increased hospitalization rates and higher healthcare costs [8]. Research indicates that middle-aged individuals with COPD face nearly double the risk of developing dementia in later life compared to the general population [9]. Smoking is recognized as a risk factor for dementia, a condition primarily characterized by progressive cognitive decline [10]. Animal studies further demonstrate that CS exposure severely impairs learning and memory in rodents [5, 11]. For instance, one study showed that CS exposure alters microglial morphology and volume in the mouse hippocampus, impairing working memory maintenance [12]. These microglia exhibit a more active morphology. Additionally, mice exposed to CS exhibit changes in astrocyte density, along with reductions in synaptophysin and dendritic spines within the hippocampus [13]. Although it is widely believed that chronic COPD is caused by CS and is associated with neurocognitive function [14], the underlying mechanism remains unclear.

Existing studies have shown that damage to the airway epithelial barrier is an important feature of COPD [15]. The inflammation induced by CS can disrupt the connections between adjacent epithelial cells, increasing the permeability of the epithelium, thereby leading to lung injury caused by inhaled particles and infection [16]. At the same time, the increase in epithelial permeability also leads to the "spill-over" of inflammatory factors from the lungs into the blood circulation, which may play a key role in the pathogenesis of COPD and its complications [17, 18]. For example, in in vivo models, CS can induce the permeability of airway mucosa and instantly destroy the epithelial barrier function in vitro models, thereby disrupting the connections and expressions of occluding (OCLN) and zonula occludens (ZO)-1 [19]. Among them, the triad of pro-inflammatory cytokines (TNF-α, IL-6, IL-1β) are most likely to cause barrier dysfunction in COPD and jointly contribute to barrier dysfunction through different mechanisms: (1) TNF-α promotes the internalization of Src-dependent E-cadherin [20]; (2) IL-1β triggers neuregulin (NRG)-1 shedding mediated by a disintegrin and metalloproteinase (ADAM) 17, which leads to the dissociation of intercellular β-catenin-E-cadherin adhesion complexes and the reduction of barrier function [21]; (3) IL-6 enhances the dissociation of β-catenin driven by HER2, thereby destroying the integrity of airway epithelium [22].

Meanwhile, there might exist a bidirectional communication network between the lungs and the brain, known as the lung-brain axis. This axis covers various pathways such as the humoral (cytokines, metabolites), neural (vagal afferents), and cellular (monocyte trafficking) pathways [23]. As we have previously discussed, when chronic CS stimulation leads to an increase in the permeability of the airway epithelial barrier, pro-inflammatory factors may "spill-over" into the bloodstream, leading to secondary diseases in the CNS [24]. The physical barrier that separates the CNS from the bloodstream-the blood-brain barrier (BBB) will be the first site where these inflammatory factors are stimulated [25]. The BBB is highly sensitive to inflammatory stimuli and peripheral inflammation can disrupt the integrity of the BBB by down-regulating tight junction proteins and up-regulating adhesion molecules [26]. Subsequently, the infiltration of inflammatory factors promotes the activation of microglia, thereby exacerbating neuroinflammation [27]. Neuroinflammation is the link between long-term neurological damage and brain dysfunction, leading to various cognitive complications and behavioral symptoms [28]. These studies suggest that in patients with COPD-NCDs, the changes in the permeability of the lung barrier and the BBB, the overflow of inflammatory factors, and neuroinflammation are seemingly associated with cognitive dysfunction in an inevitable manner.

Critically, while CS is known to disrupt both lung and BBB barriers, the causal relationship between lung-derived inflammatory "spill-over" and hippocampal dysfunction remains unestablished. We propose that

CS disrupts lung-brain barriers, enabling inflammatory "spill-over" to drive hippocampal dysfunction. Herein, we integrate two-sample Mendelian randomization (MR) with longitudinal murine models and single-cell RNA sequencing (scRNA-seq) to: (1) Establish causal links between COPD duration and cognitive decline; (2) Delineate lung-brain axis pathophysiology; (3) Identify BBB-specific therapeutic targets.

Materials and methods

Two-sample MR

We conducted two-sample MR analyses in compliance with STROBE-MR guidelines [29], employing five complementary methods: MR Egger (MR), weighted median estimator (WME), inverse variance weighted (IVW), simple mode (SM), and weighted mode (WMO). All two-sample MR results and integrated data are shown in Table S1-1 and Table S1-2.

Animals

Female BALB/c mice (age: 6 weeks; weight: 18–22 g) were obtained from Changchun Yisi Laboratory Animal Technology Co. Ltd (License No. SCXK 2020–0002) and maintained under specific pathogen free (SPF) conditions with ad libitum access to food and water. All protocols involving animal experiments in this research were approved by the Ethics Committee for Animal Experiments of the College of Basic Medical Sciences of Jilin University (Approval No.2025–361), and were performed in accordance with the National Institutes of Health Guide for the Care and Use of Laboratory Animals.

CS exposure

Mice were acclimatized for 1 week before the start of the experiment and randomly assigned to different experimental groups ($n = 30$/group). Body weights were recorded every week. Mice received twice daily exposures to either CS generated from commercial filtered cigarettes (tar: 10 mg/cigarette; nicotine: 0.9 mg/cigarette; CO: 11 mg/cigarette) or filtered air (control). CS exposed mice were exposed to 9 whole cigarettes/day, 5 days per week, for 24 weeks. After 22 weeks of CS exposure (2 weeks prior to culling), the mice were subjected to neurocognitive testing and pulmonary function testing. Blood samples were collected from the retro-orbital plexus, and the animals were then necropsied, and lung and brain tissue were collected for further study.

Measurement of lung function

Invasive lung function test

According to the methods from previous studies, lung function indicators were measured in six mice per group [30]. Briefly, invasive lung function tests were conducted using the Buxco pulmonary function testing system (ST. PAUL, MN, USA). Each mouse was deeply anesthetized, secured in position, and an endotracheal tube was inserted for mechanical ventilation. After respiration stabilized, the spirometer automatically recorded the lung function parameters.

Non-invasive lung function test

The airway function parameters of conscious and spontaneous breathing mice ($n = 6$/group) were measured with the help of a mouse whole-body plethysmograph (WBP, #WBP-4 M). Further analysis of respiratory parameters includes inspiratory time (Ti), expiratory time (Te), peak inspiratory flow (PIF), peak expiratory flow (PEF), expiratory flow at 50% tidal volume (EF50), and minute ventilation (MV).

Behavioral tests

A cohort of eight mice per group underwent the open field (OF) test, the novel object recognition (NOR) test, and the Morris water maze (MWM) test sequentially. Before testing, the mice were acclimatized to the testing room environment. Each behavioral test was conducted over several consecutive days using the same group of mice.

OF test

The OF test was conducted in a rectangular box (60 cm × 60 cm × 60 cm). Mice were quickly placed in the center area of the experimental box, and the tracking software was turned on to automatically record the mice's behavior inside the box for 10 min. The box was wiped between each set of tests to remove any residual odor from the mice. The following data were collected using the tracking software: time to center movement, distance to center movement, total distance traveled.

NOR test

Mice were acclimated for 5 min in an open-field arena (60 cm × 60 cm × 60 cm). For training, two identical cylindrical objects (diameter: 5 cm; height: 5 cm) were placed in diagonally opposite corners, allowing 10 min of free exploration. After 24 h, one of the cylinders is replaced with a cone (length, width and height: 5 cm each). During the testing stage, the mice were allowed to explore freely for 10 min and were permitted to interact with and recognize the new object. The time when animals made physical contact with and sniffed objects was regarded as exploration time. The retention time of new objects and the discrimination index during the test stage were recorded.

MWM test

The MWM test was conducted in an independent laboratory to ensure a quiet environment and to avoid

interference with the experimental subjects. A platform with a diameter of 12 cm was placed two centimeters below the water surface, at the center of the third quadrant (in situ). The water pool was divided into four quadrants, each with walls labeled with different symbols (triangles, circles, pentagrams, and squares) to provide additional spatial cues to the maze. The water temperature was maintained at 23 ℃ ± 1 ℃, and all water maze experiments were conducted at the same time point each day. Mice were conditioned in the water maze chamber for 2 h before the experiment. Each mouse undergoes 5 days of training, with two tests conducted each day, with an interval of 4 h between each test. Mice were gently placed in a certain quadrant of the pool without human interference, facing away from the pool wall. During training process, if the mouse found the platform for more than 60 s, it would be guided to the platform and stayed there for 10 s. The mouse was then moved to the platform, and the platform was removed from the pool. After 24 h of training, the platform was removed and the 60 s exploration test began. Mice were placed in the pool, facing the area opposite the target quadrant. The time spent in the target quadrant and the time taken to reach the platform position were recorded as indicators of spatial memory.

Histological examination

Remove the lungs and brain ($n = 4$/group) and fix them in 4% paraformaldehyde. Tissue sections were prepared after paraffin embedding. Lung sections were stained with hematoxylin/eosin (HE) (Beyotime, Cat#C0105S) and Masson (Servicebio, Cat#G1006). Brain slices were stained with HE.

Enzyme-linked immunosorbent assay (ELISA)

Tissues were homogenized in ice-cold PBS (1:10 w/v) using a mechanical homogenizer, followed by centrifugation at 3,000 × g for 5 min at 4 °C. The resulting supernatant was aliquoted for subsequent assays. The levels of IL-1β, IL-6, TNF-α and CCL3 in the supernatant and mice serum ($n = 6$/group) were measured using an ELISA kit (ColorfulGene Biotech, China) according to the manufacturer's protocol.

Table 1 List of antibodies for immunofluorescent chemical staining

Antibody	Species	Manufacturers	Concentration
GFAP	Mouse	Sigma	1:300
IBA1	Chicken	Synaptic Systems	1:500
Neun	Rat	Abcam	1:200
Synaptophsin	Rabbit	Abcam	1:200
Occludin	Rabbit	Proteintech Group	1:200
Claudin	Rabbit	Proteintech Group	1:200
ZO1	Mouse	Proteintech Group	1:200

Immunofluorescence (IF)

Sections were blocked with 10% normal goat serum for 20 min at room temperature, followed by overnight incubation at 4 °C with the following primary antibodies (Table 1):

The next day, after being placed at room temperature for 30 min, the slices were combined with the fluorescent Goat anti-rabbit IgG H&L (1:500, invitrogen) secondary antibody for 2 h. The cell nucleus was re-stained with DAPI or Hoechst. Images were obtained by fluorescence microscopy (Olympus BX53, Japan) and the image data were processed by the ImageJ software package.

ScRNA-seq

Mice were anesthetized by intraperitoneal injection of 1% sodium pentobarbital, and sterile PBS was infused from the left ventricle to remove circulating blood cells from the tissues. Single-cell RNA sequences were obtained from whole brains of NC versus COPD-NCDs mice ($n = 3$/group). Tissues were digested with enzymes and processed into single-cell suspensions. Cells that met quality control were strictly followed by 10-fold Genomics SOPs for library construction and quality control. We removed dead cells and adjusted the cells to the desired concentration and detected approximately 7000 cells on the machine. On-machine sequencing was performed using the Illumina NovaSeq 6000 PE150 sequencing strategy. Bioinformatics analysis was performed using the BMKCloud (www.biocloud.net).

Real-time quantitative polymerase chain reaction (RT-qPCR)

Total RNA was extracted from lung and brain tissues ($n = 6$/group) using TRIzol reagent (Tiangen Biotech, Cat#DP424). Complementary DNA was synthesized using a cDNA reverse transcription kit (Applied Biological Materials, Cat#G592) according to the manufacturer's instructions. RT-qPCR was performed using FastStart Universal SYBR Green Master premix (Sigma-Aldrich, Cat#04913914001) and Fast qPCR System (Applied Biosystems, USA). Gene expression was quantified via the 2−ΔΔCt method. The primers used in this study are listed in Table S2.

Western blotting

Total protein was extracted from lung and brain tissue ($n = 6$/group) using RIPA lysis buffer containing protease inhibitors and deacetylase inhibitors. Protein-containing lysates were mixed with SDS-PAGE sample buffer, 37 ℃ for 30 min, separated by SDS-PAGE, and transferred to PVDF membranes. After sealing with protein free rapid sealing solution (Servicebio, Cat#G2052-500 ml), the membrane was incubated with primary antibody at 4 ℃ overnight with gentle shaking. Primary antibodies

used were: Anti-Occludin (1:10000, Proteintech Group), Anti-ZO-1 (1:20000, Proteintech Group), Anti-Claudin1(1:1500, Affinity Biosciences) and Anti-β-Actin (Proteintech Group, Cat#20536-1-AP). After incubation, HRP-coupled goat-anti-rabbit IgG (1:5000, Immunoway) was added and incubated for 1 h at room temperature. Protein bands were detected using enhanced chemiluminescence (ECL) substrate and quantified with ImageJ software.

Evaluation of Evans blue (EB) leakage

The barrier permeability of the lungs and brain ($n = 6$/group) was measured using EB. In brief, after pentobarbital sodium anesthesia, each group of mice was injected with 2% EB (5 ml/kg) via the tail vein. Two hours later, the mice were perfused with PBS through the left ventricle. The lung and brain tissues were excised and homogenized in dimethyl sulfoxide. The mixture was incubated at 50 ℃ for 2 h. Then, the homogenate was centrifuged at 12000 g for 30 min and the absorbance was measured at 620 nm on a Microplate Reader (Biotek Epoch, USA).

Statistical analysis

All statistical analyses were performed using GraphPad Prism software (version 8.0) and R (version 4.3.2). Continuous data are expressed as means ± standard deviation (SD), with individual sample sizes (n values) specified in corresponding figure legends. For comparisons between two groups, we employed unpaired two-tailed Student's T-tests after confirming normality (Shapiro-Wilk test) and homogeneity of variance (F-test). Multiple group comparisons were performed using one-way ANOVA followed by Tukey's post hoc test for normally distributed data. A p-value of < 0.05 was considered statistically significant in all statistical methods. The standard symbols were presented as $^{*}P < 0.05$, $^{**}P < 0.01$, $^{***}P < 0.001$, and $^{****}P < 0.0001$.

Results

Clinical correlations between COPD patients and neurocognitive disorders

Using two-sample MR analysis with genetic indicators from the IEU GWAS database, we investigated the association between COPD (categorized by disease stages: early, hospitalized, and late-phase) and neurocognitive disorders (including dementia, Alzheimer's disease, Parkinson's disease, anxiety and depression). All analyses accounted for multiplicity (Table S1-4) and heterogeneity (Table S1-5), with GWAS summary statistics detailed in Table S1-3. Notably, early-stage COPD (COPD_EARLY) showed significant associations with: Alzheimer's disease (OR_{IVW} = 1.000255, 95%CI = [1.000025, 1.000486], $P = 0.030$; OR_{WME} = 1.000414, 95%CI = [1.000076, 1.000752], $P = 0.016$;), Dementia (OR_{WEM} = 1.0939, 95%CI = [1.0144, 1.1797], $P = 0.0197$), and Depression (OR_{IVW} = 1.00195, 95%CI = [1.00082, 1.00307], $P = 0.00068$; OR_{MR} = 1.00275, 95%CI = [1.00062, 1.00488], $P = 0.0159$; OR_{WME} = 1.00223, 95%CI = [1.00059, 1.00387], $P = 0.0077$; ORWMO = 1.00243, 95%CI = [1.00012, 1.00474], $P = 0.047$). Late-stage COPD (Finn-b-COPD_LATER) demonstrated stronger effects on Anxiety (OR_{IVW} = 1.57, 95%CI = [1.17, 2.12], $P = 0.0026$; OR_{MR} = 1.99, 95%CI = [1.13, 3.51], $P = 0.032$; OR_{WME} = 1.61, 95%CI = [1.07, 2.43], $P = 0.024$; OR_{WMO} = 2.00, 95%CI = [1.22, 3.27], $P = 0.014$). Hospitalized COPD patients showed elevated Parkinson's disease risk (OR_{IVW} = 1.60, 95%CI = [1.16, 2.20], $P = 0.004$).

The dose-response pattern suggests progressively stronger associations with neurocognitive disorders as COPD duration increases, though the absolute effect sizes for early-stage associations were modest (Fig. 1A). Sensitivity analyses using MR-Egger and IVW (Fig. 1B-G) showed consistent directions of effects. In conclusion, large-scale GWAS data demonstrated that COPD is a significant risk factor for neurocognitive dysfunction. In the clinical setting, there is a great need to focus on whether cognitive function is impaired in patients with COPD, especially in advanced stages, in order to determine the right clinical intervention strategies.

CS exposure induces a COPD phenotype in mice

To establish a COPD mouse model, BALB/c female mice were exposed to CS (9 whole cigarettes/day, 5 days per week) for 24 weeks (Fig. 2A). Compared to the normal control (NC) group, CS-exposed mice exhibited reduced body weight gain (Fig. 2B), with significantly lower final weight at week 24 (21.61 ± 2.91, $P < 0.001$) (Fig. 2C).

Figure 2D and F show the invasive pulmonary function indicators of mice, including FEV0.1 (forced expiratory volume in 100ms)/FVC (forced vital capacity), RI (airway resistance) and Cydn (dynamic compliance). Compared with the NC group, the pulmonary function of mice in the COPD-NCDs deteriorated: decreased FEV0.1/FVC (0.53 ± 0.11, $P < 0.0001$), increased RI (6.44 ± 1.99, $P < 0.05$), and reduced Cydn (0.007 ± 0.002, $P < 0.05$). We also performed noninvasive lung function tests in mice, and the six indices of Ti, Te, PIF, PEF, MV, and EF50 also illustrated the reduced lung function in the COPD-NCDs group of mice compared to the NC group (all $P < 0.05$, Fig. 2G and L). ELISA results showed that the levels of inflammatory factors IL-1β (61.89 ± 5.52, $P < 0.01$), IL-6 (81.69 ± 7.43, $P < 0.001$) and TNF-α (249.96 ± 14.6, $P < 0.001$) were significantly elevated in lung tissues (Fig. 2M and O). Pulmonary emphysema formation (Fig. 2P) and airway surrounding collagen deposition (Fig. 2Q) were also observed in the lungs of the COPD mouse model. These data confirm successful induction of

A

Exposure	Outcome	method	nsnp	pval
COPD_EARLY	Alzheimer's disease	Inverse variance weighted	35	0.030055468
COPD_EARLY	Alzheimer's disease	MR Egger	35	0.084206762
COPD_EARLY	Alzheimer's disease	Weighted median	35	0.016495476
COPD_EARLY	Alzheimer's disease	Weighted mode	35	0.116092930
COPD_EARLY	Dementia	Inverse variance weighted	37	0.054148280
COPD_EARLY	Dementia	MR Egger	37	0.084778954
COPD_EARLY	Dementia	Weighted median	37	0.019739867
COPD_EARLY	Dementia	Weighted mode	37	0.080391531
COPD_EARLY	Depression	Inverse variance weighted	36	0.000683837
COPD_EARLY	Depression	MR Egger	36	0.015944434
COPD_EARLY	Depression	Weighted median	36	0.007718565
COPD_EARLY	Depression	Weighted mode	36	0.047120459
COPD_HOSPITAL	Parkinson's disease	Inverse variance weighted	8	0.004432906
COPD_HOSPITAL	Parkinson's disease	MR Egger	8	0.461107048
COPD_HOSPITAL	Parkinson's disease	Weighted median	8	0.069532908
COPD_HOSPITAL	Parkinson's disease	Weighted mode	8	0.306029585
COPD_LATER	Recent feelings or nervousness or anxiety	Inverse variance weighted	17	0.011178091
COPD_LATER	Recent feelings or nervousness or anxiety	MR Egger	17	0.872671980
COPD_LATER	Recent feelings or nervousness or anxiety	Weighted median	17	0.297512083
COPD_LATER	Recent feelings or nervousness or anxiety	Weighted mode	17	0.607386783
COPD_LATER	Seen doctor for nerves, anxiety, tension or depression	Inverse variance weighted	16	0.002642511
COPD_LATER	Seen doctor for nerves, anxiety, tension or depression	MR Egger	16	0.032146751
COPD_LATER	Seen doctor for nerves, anxiety, tension or depression	Weighted median	16	0.023812900
COPD_LATER	Seen doctor for nerves, anxiety, tension or depression	Weighted mode	16	0.014477016

P<0.05 was considered statistically significant

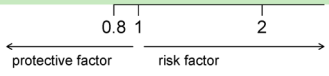

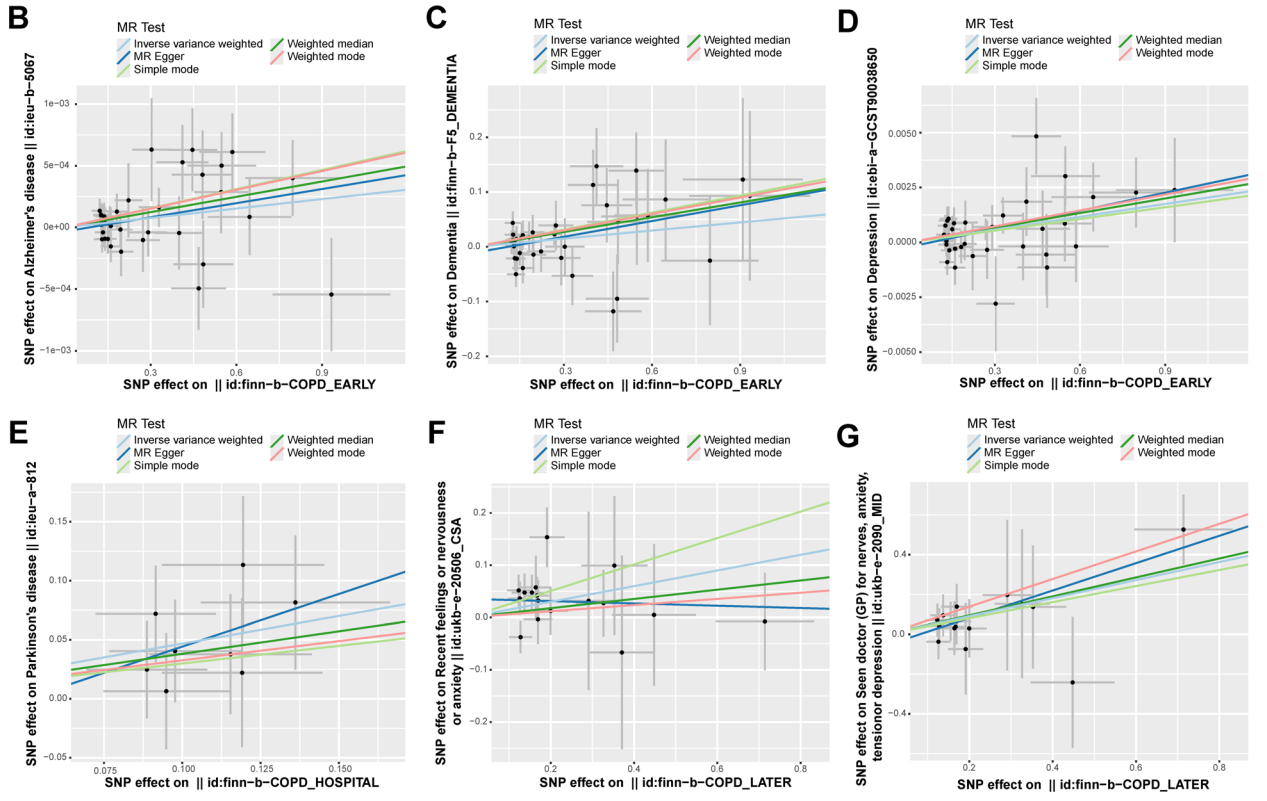

Fig. 1 Two-sample MR analysis of COPD and neurocognitive disorders. **A** Results of the causal relationship between COPD (early, hospital, and later) and neurocognitive disorders (dementia, Alzheimer's disease, Parkinson's disease, anxiety and depression). **B**-**G** Scatter plots of the causal relationship between COPD and neurocognitive disorders using different MR methods

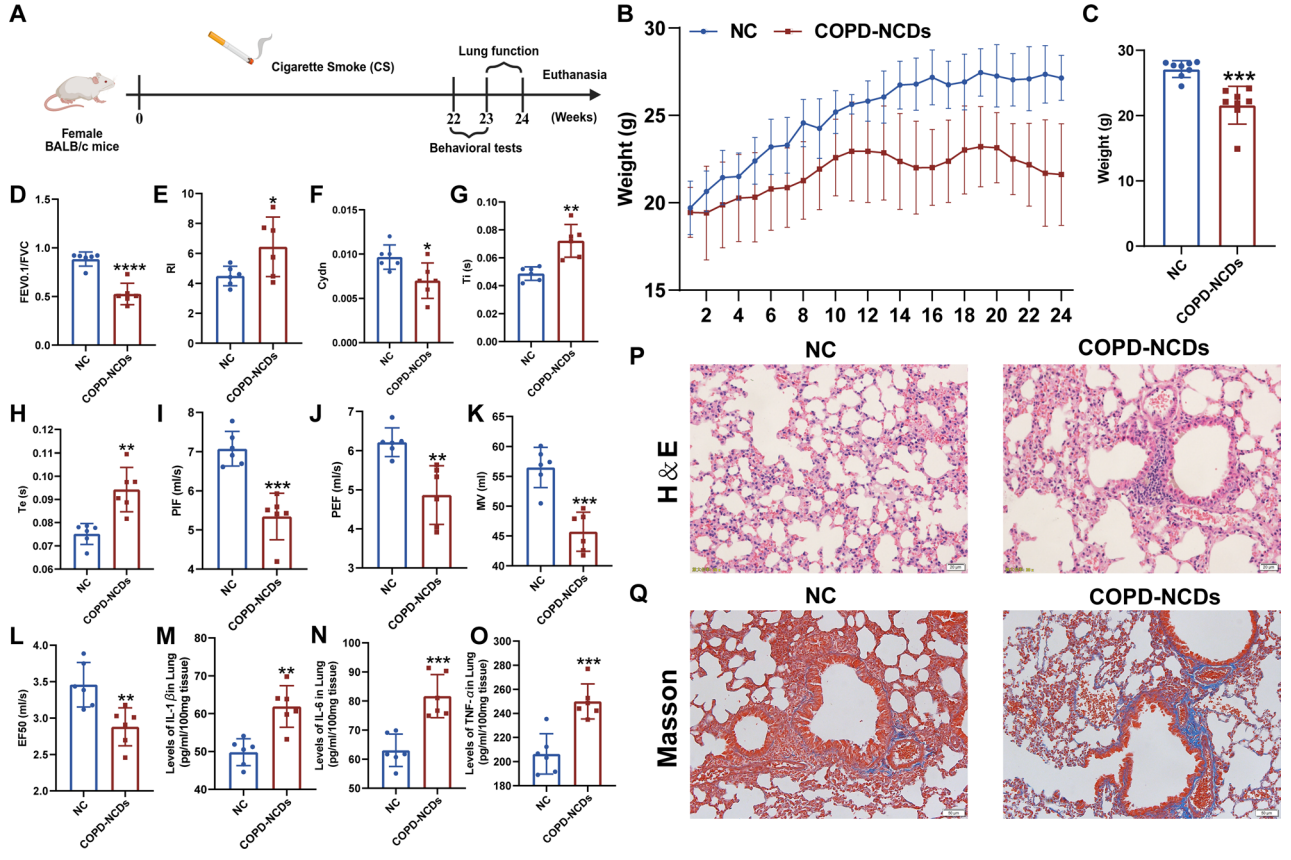

Fig. 2 Chronic CS exposure worsened lung function. **A** Molding process for COPD-NCDs mouse models. **B** 24-Week mouse body weights. **C** A comparison of weights in the 24th week; ($n=8$) in each group. Invasive lung function testing was carried out with FEV0.1/ FVC (forced expiratory volume in 100 ms/ forced vital capacity), RI (airway resistance) and Cydn (dynamic compliance) shown in **D**-**F**, respectively ($n=6$/group). **G**-**L** Noninvasive pulmonary function tests were performed, Ti, Te, PIF, PEF, MV, and EF50 ($n=6$/group). **M**-**O** Levels of inflammatory factors IL-1β (M), IL-6 (N), and TNF-α (O) in lung tissue homogenate, measured by ELISA ($n=6$ mice/group). **P** HE staining of pulmonary tissue of mice ($n=4$/group) (scale bar = 100 μm). **Q** MASSON staining of pulmonary tissue of mice ($n=4$/group) (scale bar = 100 μm). Statistical significance was determined by Student's t-test. $^{*}P<0.05$, $^{**}P<0.01$, $^{***}P<0.001$ and $^{****}P<0.0001$ compared with the NC group

COPD-like phenotypes in mice, mimicking human disease progression.

CS exposure induces working memory deficits and hippocampal neuroinflammation

To investigate whether chronic CS-induced COPD and cognitive dysfunction are related, we subjected mice to behavioral tests after 22-week CS exposure. In the OF test, the COPD-NCDs mice exhibited anxiety-like behaviors (more huddled in the corner and immobile), with reduced total activity path (COPD-NCDs group: 839.86 ± 262.12 vs. NC group: 2239.99 ± 732.43, $P<0.001$), central zone entries (COPD-NCDs group: 135.3 ± 40.6 vs. NC group: 340.11 ± 72.39, $P<0.0001$), and central activity time (COPD-NCDs group: 16.21 ± 6.06 vs. NC group: 46.89 ± 6.95, $P<0.0001$) (Fig. 3A, D and G). In the NOR test, COPD-NCDs mice showed lower preference index for novel objects (COPD-NCDs group: 0.27 ± 0.08 vs. NC group: 0.54 ± 0.11, $P<0.0001$), indicating impaired cognitive ability and short-term memory (Fig. 3B and C). The MWM was used to assess the effects of CS exposure on cognitive function in mice. The representative tracking results of the MWM tests in each group involved in the probe trial are shown in Fig. 3H. After 24 weeks of CS exposure, the mice with COPD-NCDs showed a significant prolongation of the latency of their escape response after 5 days of training (Fig. 3I). On the test day, the frequency (1.38 ± 0.92, $P<0.01$) and duration (25.25 ± 9.03, $P<0.0001$) of the COPD-NCDs mice crossing the target area platform were both lower (Fig. 3J and K).

Inflammatory factors IL-1β (65.25 ± 10.87, $P<0.01$), IL-6 (101.78 ± 19.72, $P<0.05$) and TNF-α (209.6 ± 64.27, $P<0.01$) were significantly elevated in Hippocampal tissue (Fig. 3L and N). HE staining was then used to observe histopathologic changes in the hippocampus. As shown in Fig. 3O, the hippocampal tissue of NC mice has a layered structure with clear cell boundaries, regular and intact neuronal morphology, and clearly visible neural fiber structures. However, in the mice with COPD-NCDs, it was observed that some hippocampal neurons

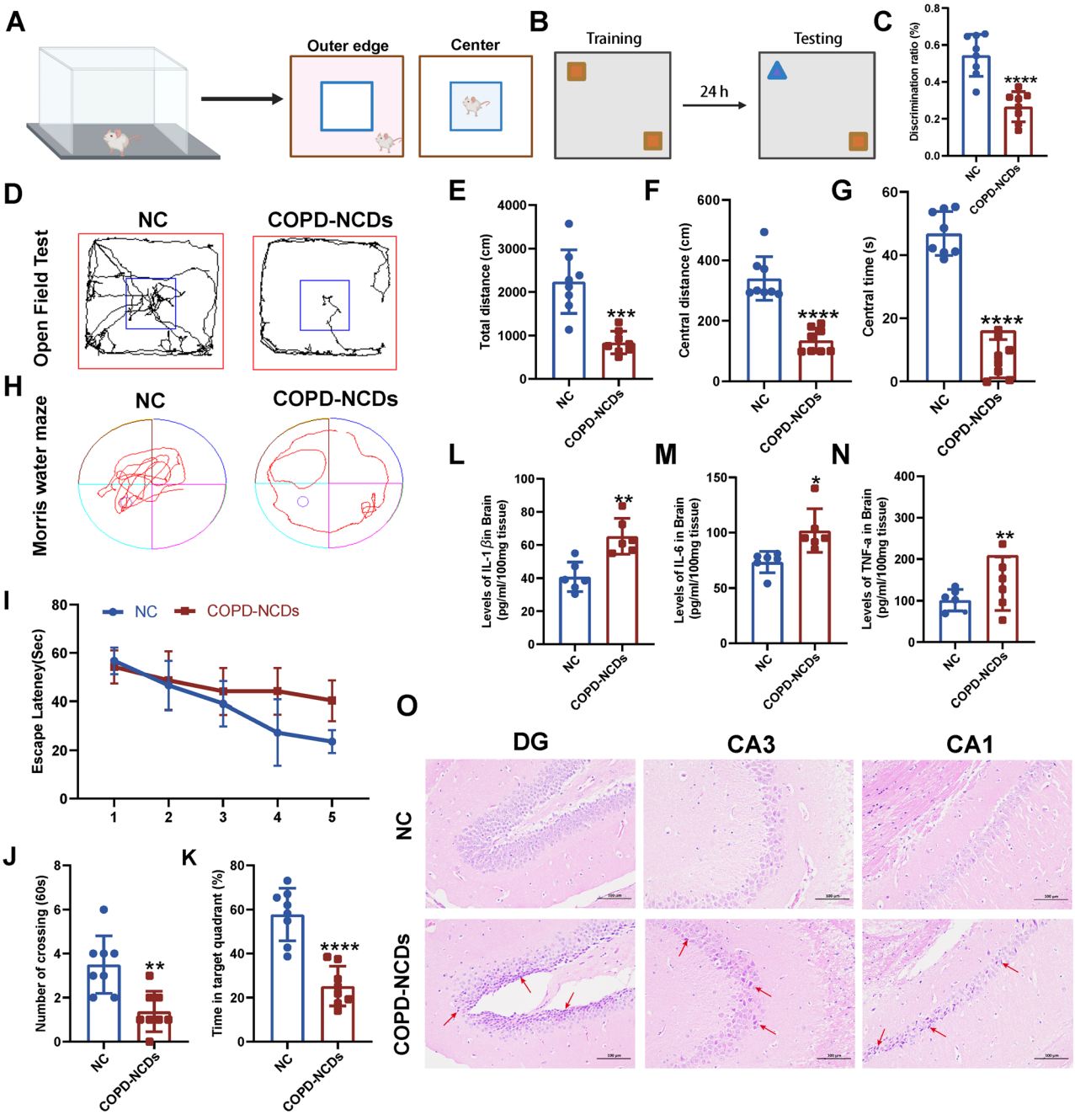

Fig. 3 CS exposure induces neurocognitive disorders in mice. **A** Schematic illustration of the OF test ($n=8$/group). **B** Schematic illustration of the NOR test ($n=8$/group). **C** Discrimination ratio in the NOR ($n=8$/group). **D** Representative paths of mice in the OF test. **E** Total distance for mice in the OF test ($n=8$/group). **F** Central distance for mice in the OF test ($n=8$/group). **G** Central time for mice in the OF test ($n=8$/group). **H** Representative plot of MWM images ($n=8$/group). Record data related to learning and memory performance including escape latency (**I**), Number of crossing (**J**), time in target quadrant (**K**) ($n=8$/group). (**L**-**N**) Inflammatory factors including IL-1β (**L**), IL-6 (**M**), and TNF-α (**N**) of brain tissue homogenate ($n=6$/group). **O** HE staining of hippocampus tissue of mice ($n=4$/group) (scale bar = 100 μm). Statistical significance was determined by Student's t-test. $^{*}P<0.05$, $^{**}P<0.01$, $^{***}P<0.001$ and $^{****}P<0.0001$ compared with the NC group

were partially absent and disorganized neuropil in CA1 and CA3. These data demonstrate that CS-induced COPD leads to hippocampal-dependent memory deficits, possibly mediated by neuroinflammation.

CS-induced neuroinflammation activates hippocampal microglia and astrocytes and triggers neuronal and synaptic dysfunction in mice

Neuroglial cell activation is often associated with neuroinflammation in neurocognitive disorders. We thus

evaluated the activation of glial cells in CS exposed mice. We used immunofluorescence to detect the expression of IBA1 protein (Fig. 4A, C and E) and GFAP protein (Fig. 4G, I and K) in the hippocampus of mice. Quantitative analysis revealed that the density of $Iba1^+$ and $GFAP^+$ in CA1 (COPD-NCDs group: 13.94 ± 3.19 vs. NC group: 5.89 ± 1.59, $P < 0.01$; COPD-NCDs group: 15.65 ± 3.44 vs. NC group: 9.43 ± 1, $P < 0.05$), CA3 (COPD-NCDs group: 16.34 ± 0.79 vs. NC group: 6.37 ± 1.57, $P < 0.0001$; COPD-NCDs group: 30.29 ± 4.01 vs. NC group: 9.91 ± 3.98, $P < 0.001$), and DG (COPD-NCDs group: 24.57 ± 1.09 vs. NC group: 7.37 ± 0.66, $P < 0.0001$; COPD-NCDs group: 13.41 ± 1.83 vs. NC group: 8.8 ± 2.37, $P < 0.05$) was significantly higher than that of the normal control group, indicating that CS-induced neuroinflammation can activate microglia and astrocytes in the hippocampus.

We further evaluated the conditions of hippocampal neurogenesis and synaptogenesis after glial cell activation. Compared to the NC group, the mature neuronal markers NeuN and synaptophysin in CA1 (6.48 ± 1, $P < 0.0001$; 6 ± 0.75, $P < 0.01$), CA3 (10.42 ± 0.61, $P < 0.01$; 11.2 ± 1.23, $P < 0.01$) and DG (12.31 ± 1.15, $P < 0.001$; 8.37 ± 1.13, $P < 0.0001$) regions in the COPD-NCDs group were significantly decreased (Fig. 5A and I), indicating neurotoxicity and synaptotoxicity. These findings demonstrate that CS exposure triggers hippocampal gliosis and subsequent neuronal dysfunction, potentially driving cognitive deficits.

ScRNA-seq reveals brain cell-type-specific alterations in COPD-NCDs

To delineate the brain microenvironment in COPD-NCDs, we performed 10x Genomics scRNA-seq sequencing on whole-brain cells from NC and COPD-NCDs mice ($n = 3$/group). First, cell clustering analysis was conducted based on the similarities among cells. The group of cells with the highest similarity was identified as a clustering unit. These clustering units were then converted into biologically meaningful cell types through cell annotation (Fig. 6C). Based on the clustering results of multiple samples, unsupervised clustering identified 19 transcriptionally distinct groups (t-SNE visualization, Fig. 6A). The clustering heatmap can comprehensively reflect the expression levels of characteristic genes of each cluster, which is an important basis for identifying marker genes. The top 10 differentially expressed genes from each cluster were selected to draw the clustering heatmap for visualization (Fig. 6B), these cluster-specific DEG (|log2FC| >0.25, $P < 0.05$) heatmaps revealed conserved gene signatures (e.g., *Plp1* in oligodendrocytes). Cells were clustered based on gene expression, and annotated into 8 major types using canonical markers (e.g., *P2ry12* for microglia, *Ptprd* for neurons),

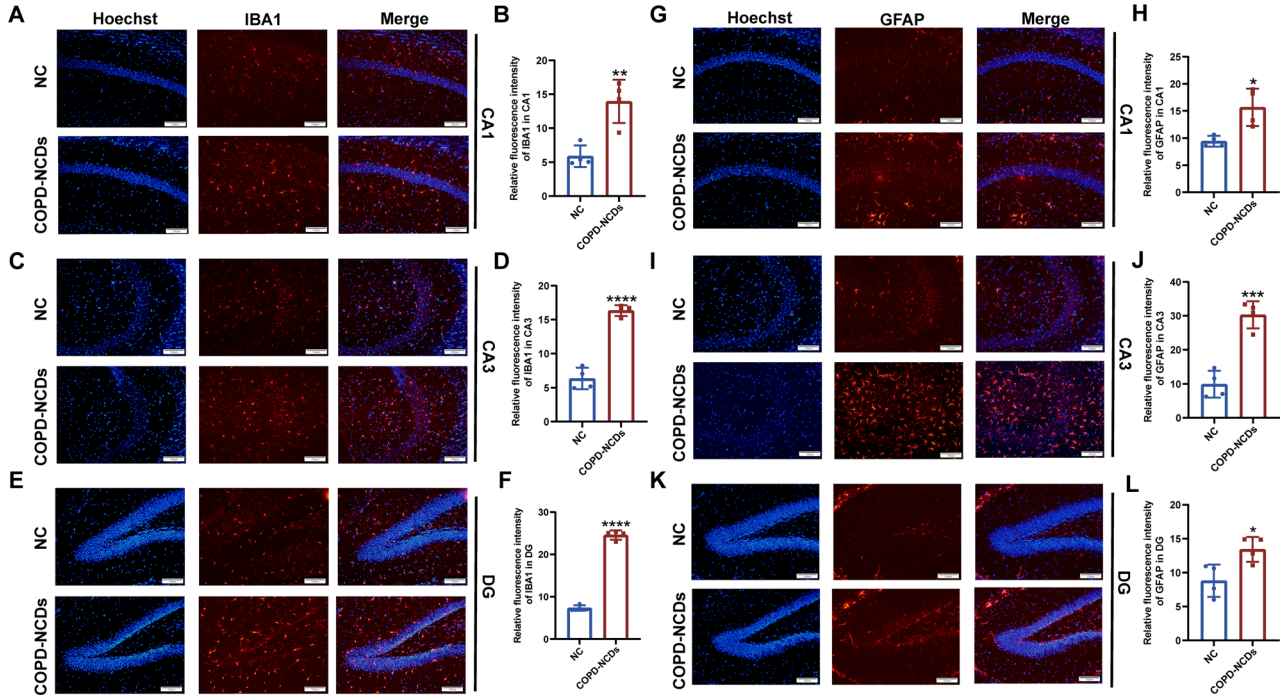

Fig. 4 Activation of microglia and astrocytes in COPD-NCDs. **A**-**F** IF staining and quantitative analysis of IBA1 in mouse hippocampal CA1, CA3 and DG regions ($n = 4$/group) (scale bar = 100 μm). **G**-**L** IF staining and quantitative analysis of GFAP in mouse hippocampal CA1, CA3 and DG regions ($n = 4$/group) (scale bar = 100 μm). Statistical significance was determined by Student's t-test. *$P < 0.05$, **$P < 0.01$, ***$P < 0.001$ and ****$P < 0.0001$compared with the NC group

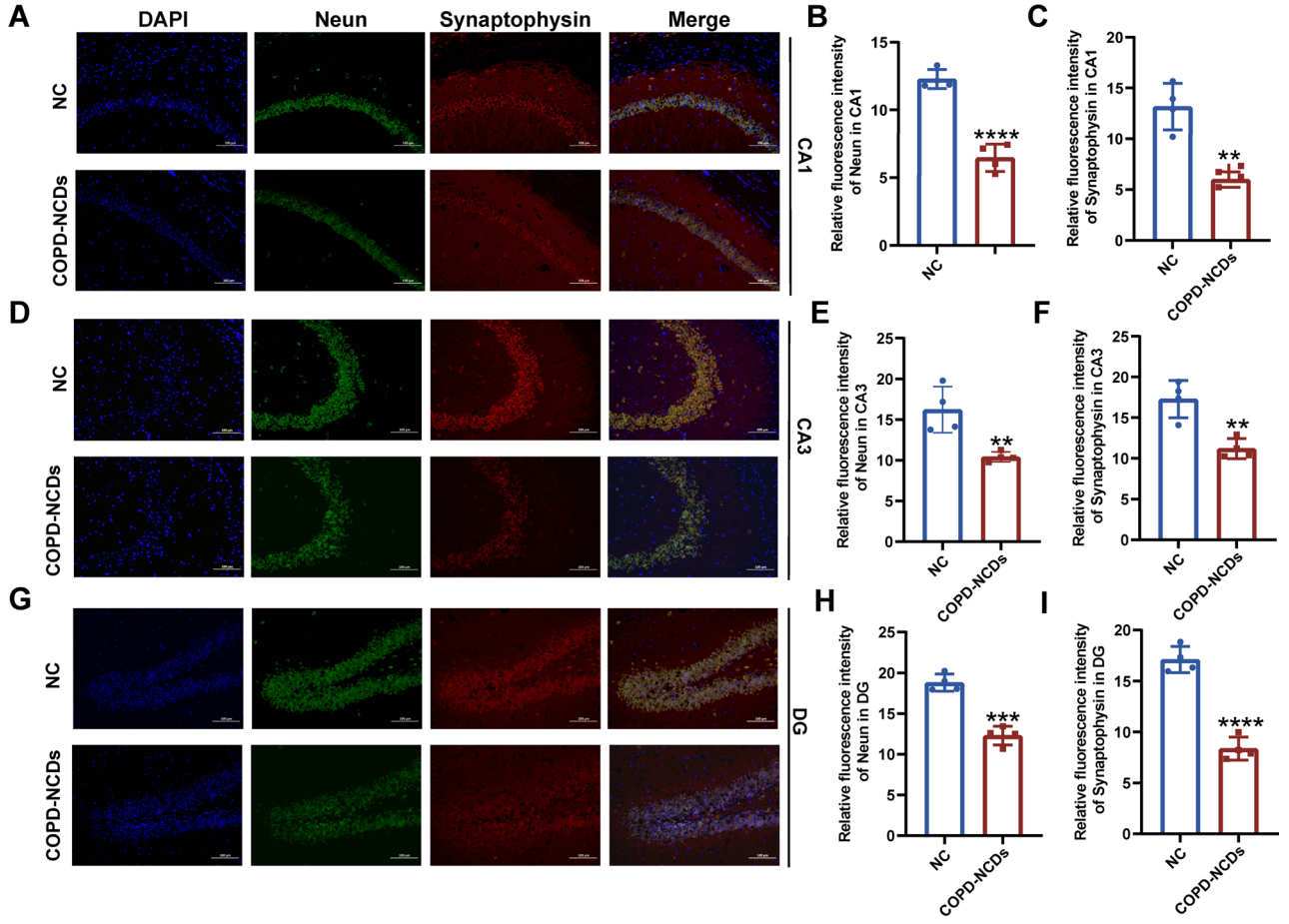

Fig. 5 Neuronal and synaptic dysfunction in COPD-NCDs. **A**, **D**, **G** Mature neurons Neun and synaptophysin IF staining in mouse hippocampal CA1, CA3 and DG regions. **B**, **E**, **H** Quantification of Neun in mouse hippocampal CA1, CA3, and DG ($n = 4$/group) (scale bar = 100 μm). **C**, **F**, **I** Quantification of synaptophysin in mouse hippocampal CA1, CA3, and DG ($n = 4$/group) (scale bar = 100 μm). Statistical significance was determined by Student's t-test. $^{**}P < 0.01$, $^{***}P < 0.001$ and $^{****}P < 0.0001$ compared with the NC group

including astrocytes, endothelial cells, ependymal, fibroblasts, microglia, neurons, OPCs and oligodendrocytes (Fig. 6D).

In NC and COPD-NCDs groups, the proportions of different cell types were shown in Fig. 6E. Endothelial cells and astrocytes are the main cell types of the BBB in the brain. Reduced proportions of endothelial cells and astrocytes, paralleled by downregulation of BBB-related genes (*Cldn5*, *Ocln*), indicating that the permeability of the BBB in the brains of COPD-NCDs mice may have changed. Bubble plots can reflect the characteristic expression of differential genes in different cells, indicating that the differential genes can serve as an important basis for the maker genes in that cell. Therefore, we specifically selected each top2 maker gene to draw bubble plots for the visualization of characteristic gene expression abundance (e.g., *Sparcl1* and *Aldoc* in astrocytes, Fig. 6F). This data provides the first evidence that COPD alters brain cellular composition, potentially through BBB dysfunction.

BBB dysfunction and synaptic impairment in COPD-NCDs

ScRNA-seq identified 143 up-regulated and 148 down-regulated DEGs in endothelial cells (the volcano plot, $|\log2FC| > 0.25$, $P < 0.05$; Fig. 7A). Gene Ontology (GO) analysis reveals significant alterations in pathways such as cell junction organization ($P = 0.0000000074$), cell migration ($P = 0.000000098$), cell motility ($P = 0.0000004$), structural molecule activity ($P = 0.0000000059$) and cell adhesion molecule binding ($P = 0.00000091$) (Fig. 7B). Kyoto Encyclopedia of Genes and Genomes (KEGG) shows that it is closely related to neurodegenerative diseases, such as Huntington disease ($P = 0.013$). In addition, it is closely related to synaptic dysfunction including Serotonergic synapse ($P = 0.014$), Glutamatergic synapse ($P = 0.026$), Dopaminergic synapse ($P = 0.039$) and Cholinergic synapse ($P = 0.028$). Besides, the enriched Gap junction ($P = 0.0000011$), Cell adhesion molecules ($P = 0.00012$) and Leukocyte trans endothelial migration ($P = 0.037$) suggest BBB disruption. PI3K-Akt signaling pathway, MAPK signaling pathway, have also been

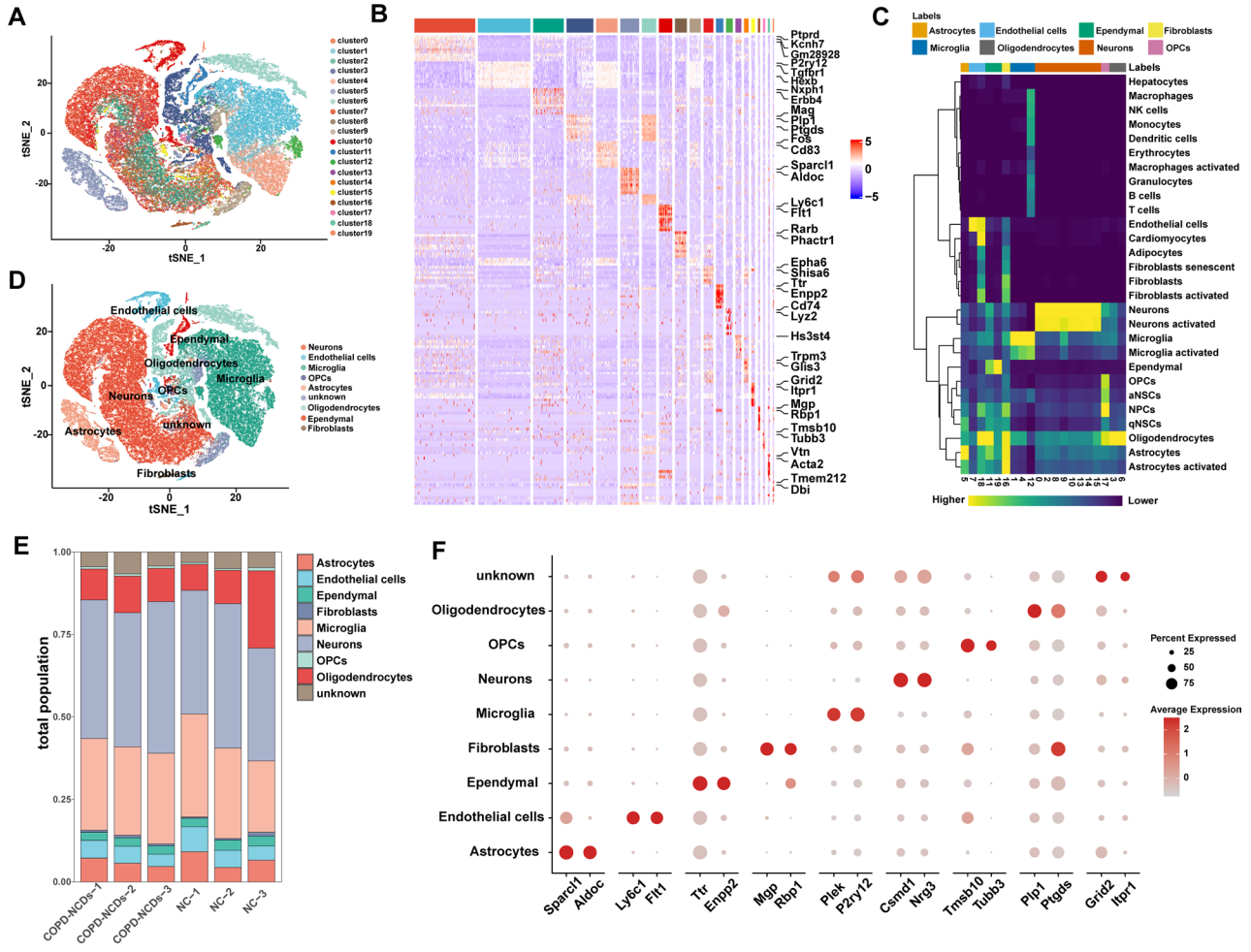

Fig. 6 The transcriptional profile of COPD-NCDs in the brain. **A** t-Distributed Stochastic Neighbor Embedding (t-SNE) showing brain cell clustering. **B** Heat maps of the top 10 gene expressions in different clusters. **C** Cell types enriched in different clusters. and (**D**) The clusters were organized into eight meta-clusters including astrocytes, endothelial cells, ependymal, fibroblasts, microglia, neurons, OPCs and oligodendrocytes. **E** The proportions of different cell types. **F** The gene dot plots of the top 2 in different cell subsets. Data are shown as means ± SD ($n = 3$/group)

significantly enriched (Fig. 7C). Studies have shown that activation of the PI3K-Akt or inhibition of P38-MAPK signaling pathway can attenuate neuroinflammation and blood-brain barrier disruption, thereby preventing/attenuating neurodegenerative diseases [31, 32]. This suggests that these two signaling pathways may be closely related to BBB and neuroinflammation in COPD-NCDs.

Similarly, in astrocytes, the volcano plot showed 119 up-regulated genes and 145 down-regulated genes (Fig. 7D). GO enrichment analysis indicated that it is closely related to nervous system development ($P = 0.000000000000000069$), synapse formation (glutamatergic synapse, ($P = 0.0000021$)), cell junction ($P = 0.0000000078$) and cell adhesion molecule binding ($P = 0.000027$) (Fig. 7E). KEGG enrichment analysis revealed a close relationship with neurocognitive disorders, such as Parkinson disease ($P = 0.033$), Long-term depression ($P = 0.014$), Huntington diseases ($P = 0.041$) and Alzheimer diseases ($P = 0.028$). Additionally, it is also closely related to pathways associated with synaptic dysfunction, such as Glutamatergic synapse ($P = 0.00034$) and GABAergic synapse ($P = 0.012$) (Fig. 7F). The gene vitrification map showed that the top 10 differentially expressed genes between endothelial cells (Ly6c1, Flt1, Itm2a, Slco1a4, Bsg, Cxcl12, Pglyrp1, Ctla2a, Slc2a1, Cldn5) and astrocytes (Sparcl1, Aldoc, Plpp3, Mt3, Atp1a2, Slc1a2, Gpr37l1, Glu, Gpc5, Ptprz1) are ranked (Fig. 7G and H). Among them, Ly6c1, Flt1, Slco1a4, Cxcl12, Slc2a1, Cldn5 and Glu, which were differentially expressed genes, were closely associated with BBB permeability. All these data indicate that dysfunction of endothelial cells and astrocytes in the brain may lead to changes in the permeability of the BBB in the brain, thereby triggering COPD-NCDs. These findings suggest that COPD-NCDs disrupt BBB integrity via endothelial-astrocyte dysfunction, exacerbating synaptic impairment.

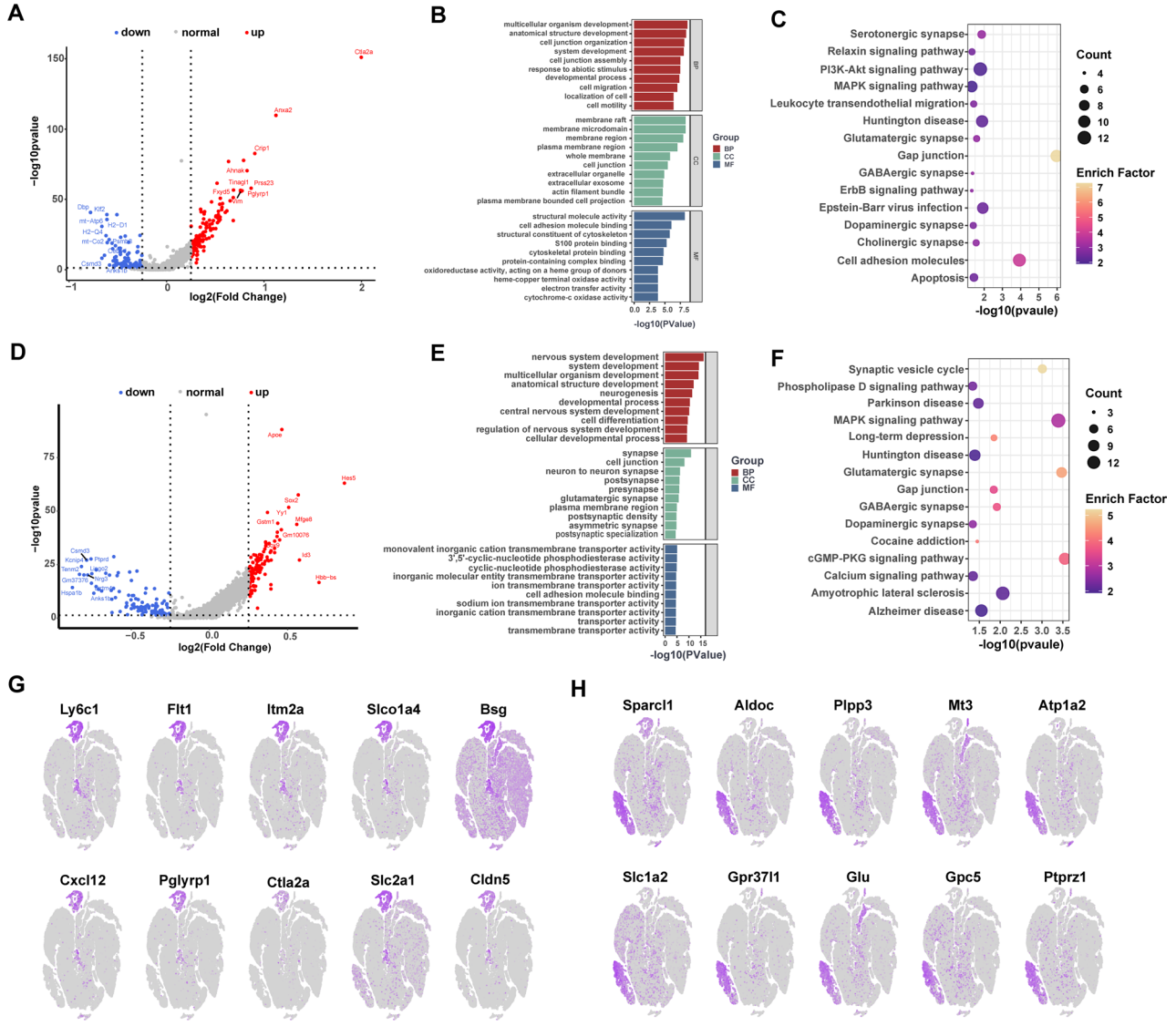

Fig. 7 Separate analysis of endothelial cells and astrocytes in COPD-NCDs. **A** A volcanic map of differentially expressed genes in endothelial cells. **B** Enrichment analysis of GO in endothelial cells. **C** Analysis of the KEGG pathway in endothelial cells. **D** A volcanic map of differentially expressed genes in astrocytes. **E** Enrichment analysis of GO in astrocytes. **F** Analysis of the KEGG pathway in astrocytes. **G** t-SNE plot of the top ten differentially expressed genes in endothelial cells. **H** t-SNE plot of the top ten differentially expressed genes in astrocytes. Data are shown as means ± SD ($n = 3$/group)

Inflammatory factors are associated with increased lung and brain permeability via translocation from the lung to the brain during COPD

Next, we attempt to determine the specific mechanism of NCDs caused by COPD. We first examined the levels of inflammatory factors such as IL-1β, IL-6, TNF-α and the chemokine CCL3 in the serum. Significantly increased expression was found in the COPD-NCDs group compared to the NC group (Fig. 8A and D): serum IL-1β (COPD-NCDs group: 71.23 ± 4.58 vs. NC group: 60.51 ± 7.9, $P < 0.05$), IL-6 (COPD-NCDs group: 108.64 ± 11.87 vs. NC group: 81.37 ± 4.06, $P < 0.001$), TNF-α (COPD-NCDs group: 453.93 ± 32.71 vs. NC group: 400.39 ± 28.84, $P < 0.05$), and CCL3 (COPD-NCDs group: 126.6 ± 4.61 vs. NC group: 111.44 ± 4.53, $P < 0.001$). Subsequently, our research investigated the tight junction proteins in the lungs and brains to elucidate the potential mechanism of transport inflammatory factors from the lungs to the brain. Our results showed that the mRNA levels and protein expression levels of Occludin, Claudin-1, and ZO-1 in the lung and brain of COPD-NCDs mice were significantly lower than those of normal mice: reduced Occludin (mRNA: lung, 2.54-fold, $P < 0.0001$, brain, 1.57-fold, $P < 0.001$; protein: lung 2.32-fold, $P < 0.0001$, brain, 1.72-fold, $P < 0.0001$), Claudin1 (mRNA: lung, 2.85-fold, $P < 0.0001$, brain, 2.89-fold, $P < 0.0001$; protein: lung 1.42-fold, $P < 0.01$, brain, 3.41-fold, $P < 0.0001$), and ZO1 (mRNA: lung, 2.72-fold,

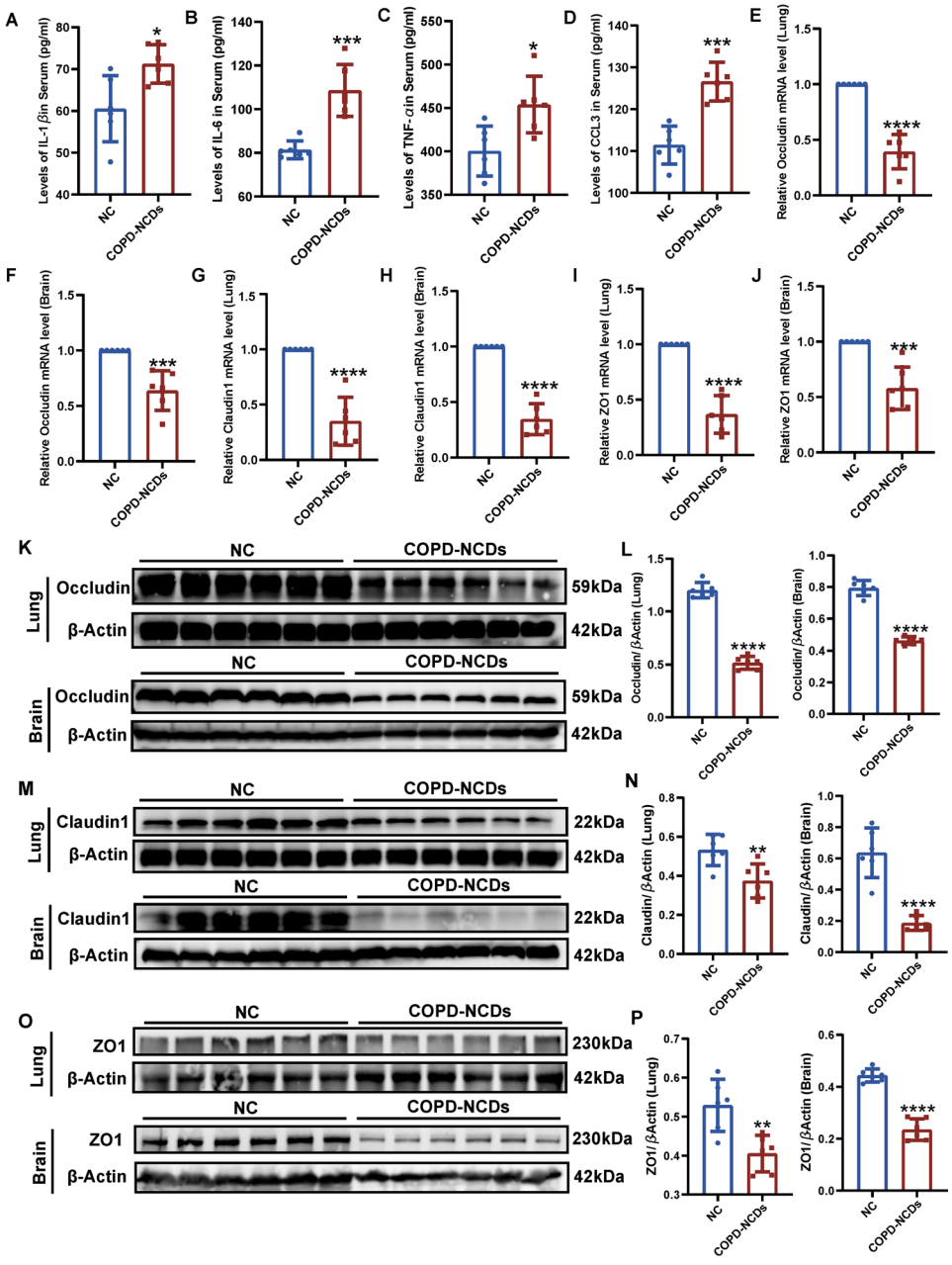

Fig. 8 Inflammatory factors cause changes in BBB permeability from the lungs to the brain. **A**-**D** Cytokine levels including IL-1β (**A**), IL-6 (**B**), TNF-α (**C**) and CCL3 (**D**) of serum ($n=6$). **E**-**J** Relative mRNA expression levels of Occludin, Claudin-1 and ZO1 in lung and brain tissues ($n=6$/group). **K**-**P** Representative Western-blot images of Occludin, Claudin1, and ZO1 proteins in lung and brain tissues with β-Actin as the internal reference ($n=6$/group). Statistical significance was determined by Student's t-test. *$P<0.05$, **$P<0.01$, ***$P<0.001$ and ****$P<0.0001$ compared with the NC group

$P<0.0001$, brain, 1.73-fold, $P<0.001$; protein: lung 1.31-fold, $P<0.01$, brain, 1.89-fold, $P<0.0001$) (Fig. 8E and P) in the lung and brain.

Further detection by IF also revealed that Occludin (lung: COPD-NCDs group: 9.97 ± 0.57 vs. NC group: 16.87 ± 0.72, $P<0.001$; brain: COPD-NCDs group: 1.83 ± 0.47 vs. NC group: 4.08 ± 0.68, $P<0.01$), Claudin1 (lung: COPD-NCDs group: 10.28 ± 0.35 vs. NC group: 18.24 ± 0.87, $P<0.001$; brain: COPD-NCDs group: 1.83 ± 0.23 vs. NC group: 3 ± 0.62, $P<0.05$) and ZO1 (lung: COPD-NCDs group: 12.3 ± 1.32 vs. NC group: 21.58 ± 0.4, $P<0.001$; brain: COPD-NCDs group: 1.83 ± 0.1 vs. NC group: 3.62 ± 0.24, $P<0.001$) were significantly lower in COPD-NCDs compared with the NC group (Fig. 9D and L). Increased EB permeability in lung (3.26-fold, $P<0.0001$) and brain (1.7-fold, $P<0.001$), confirming barrier disruption (Fig. 9A and C). This strongly suggests that the barriers between the lungs and brain,

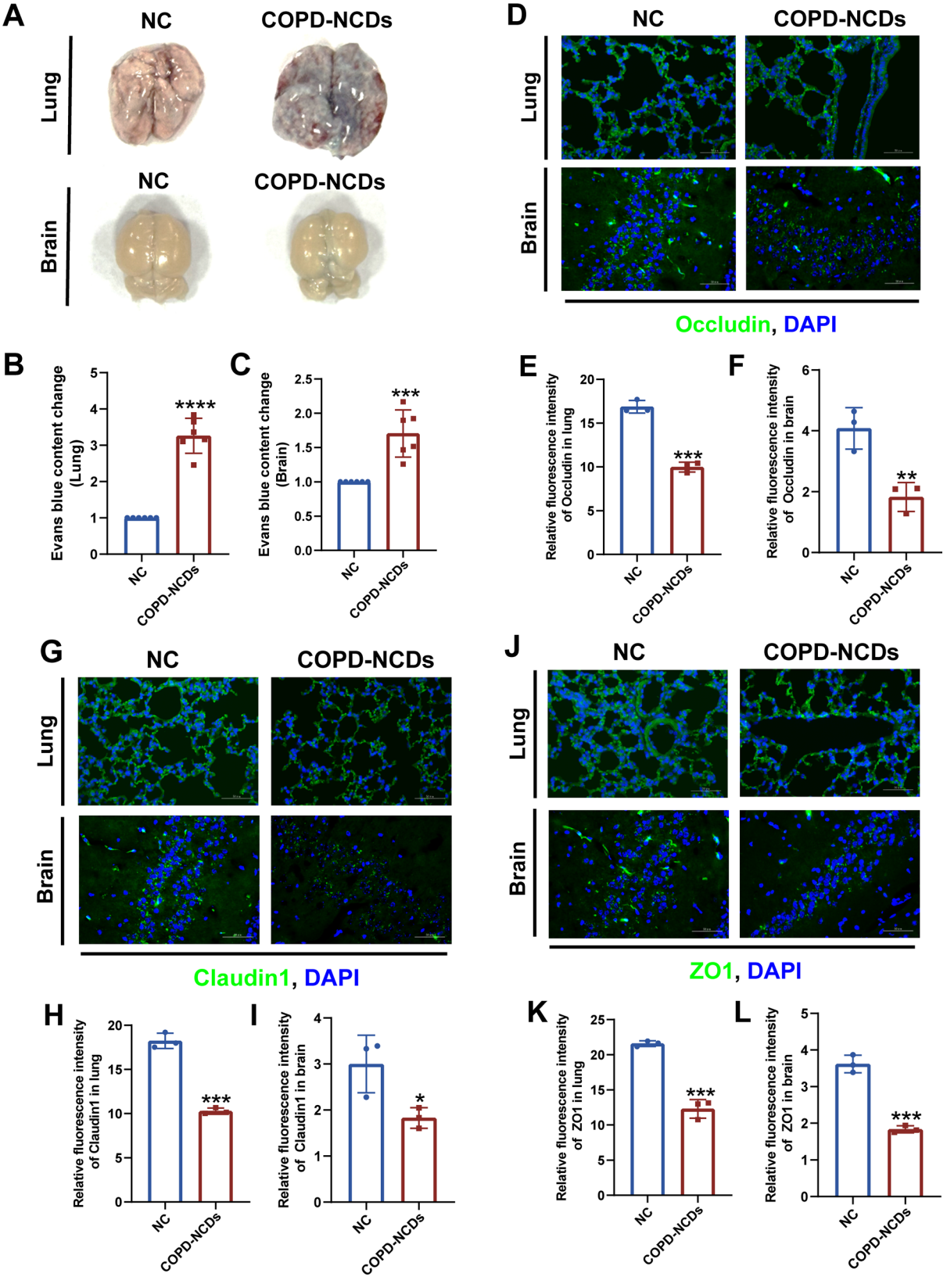

Fig. 9 (See legend on next page.)

(See figure on previous page.)

Fig. 9 The barrier functions of the lungs and the brain are impaired. **A** The images represent the EB injected lung and brain after COPD-NCDs. **B**, **C** Quantitative analysis results of EB leakage from the lung and brain ($n = 6$/group). **D**, **G**, **J** Occludin, Claudin1 and ZO1 IF staining in mouse lung and brain. **E**, **F** Quantification of Occludin in mouse lung and brain ($n = 3$/group). **H**, **I** Quantification of Claudin1 in mouse lung and brain ($n = 3$/group). **K**, **L** Quantification of ZO1 in mouse lung and brain ($n = 3$/group). Statistical significance was determined by Student's t-test. $^{*}P < 0.05$, $^{**}P < 0.01$, $^{***}P < 0.001$ and $^{****}P < 0.0001$ compared with the NC group

including the air-blood barrier and the BBB, were damaged in COPD-NCDs mice. These results support a mechanism whereby pulmonary inflammation compromises lung-brain barriers, enabling cytokine translocation to drive neuropathology, thereby influencing COPD-NCDs.

Discussion

COPD is a multi-system disorder that extends beyond pulmonary pathologies, and its impact on cognitive function is increasingly recognized [33–35]. This study adopts the MR analysis methodology referenced from our prior research. The MR Egger, WME, IVW, and Weighted mode approaches complement each other in addressing potential violations of MR core assumptions [36]. Specifically: IVW: As the foundational method utilizing all instrumental variable information, it offers the highest efficiency and serves as the primary benchmark for verification [37]. MR Egger: This method does not assume the"no horizontal pleiotropy"condition and can test for pleiotropic effects via its intercept term, thereby helping to mitigate bias [38]. WME: It provides reliable estimates when over 50% of instrumental variables are valid, offering supplementary validation when results from IVW and MR Egger diverge [39]. The limitations include: While MR can effectively reduce confounding bias, its validity relies on high-quality instrumental variables (which are vulnerable to horizontal pleiotropy and weak instrument bias). Additionally, its statistical power is often lower than that of conventional observational studies, necessitating further validation. In summary, MR analysis provides preliminary evidence on exposure-outcome relationships while reducing confounding. For the first time, through a two-sample MR analysis, we demonstrated a significant causal relationship between COPD and neurocognitive disorders, and this relationship follows a duration-dependent pattern. The longer the duration of COPD in patients, the higher the risk of neurocognitive impairment. However, studies exploring specific mechanisms underlying the association between COPD and NCDs are still relatively limited. This study elucidates a novel mechanism for cognitive dysfunction related to COPD, which may contribute to the development and optimization of therapeutic strategies for COPD-associated comorbidities.

Currently, common approaches to modeling COPD in mice include chronic CS exposure, CS combined with LPS, LPS combined with PPE, and intraperitoneal CS extract [7, 40, 41]. However, no animal model can replicate all the features of human COPD. Because CS exposure is an independent risk factor for COPD, chronic exposure to CS better reflects the pathogenesis of the disease in humans and is the most widely accepted modeling approach among researchers [24, 42]. The model is also commonly used in studies of COPD comorbidities such as cognitive dysfunction and sarcopenia [12, 43]. In our study, we chose the well-known long-term CS exposure of 24 weeks to build an animal model and assess both lung and cognitive function. Indicators of successful construction of a mouse model of COPD include lung histology showing emphysema, increased airway fibrosis and mucus secretion, reduced lung function, and elevated levels of inflammation in the lung tissue [13, 44]. 24 weeks of prolonged CS exposure is more consistent with the characteristics observed in patients with COPD. We demonstrated the validity and stability of this mouse model of COPD at the level of lung pathology.

Multiple studies have shown that COPD patients have deficits in attention, memory, learning ability and motor function [45–48]. At the neurological level, the COPD-NCDs mice in this research exhibited the following: (1) hippocampal-dependent memory deficits (NOR, MWM test); (2) anxiety-like phenotypes (OF test); (3) neuroinflammation (ELISA: IL-1β, IL-6 and TNF-α; IF: GEFP, IBA1). Our results are consistent with previous reports, that is the cognitive ability, short-term memory, and anxiety-like behaviors of COPD-NCDs mice are impaired [49]. In addition, COPD-NCDs mice had increased expression of inflammatory factors in the brain in addition to elevated lung IL-1β, IL-6, and TNF-α. COPD-NCDs mice had partial loss of hippocampal neurons and partial damage to nerve fibers. It has been suggested that the ability of CS exposure to increase lung inflammation and cause spatial and working memory deficits is due to activation of hippocampal microglia and activation of astrocyte density as well as reduction of synaptophysin in the hippocampus [12, 24]. Therefore, IF staining was used to comprehensively detect the expressions of IBA1, GFAP, Neun and synaptophysin related markers in the CA1, CA3 and DG regions of the mouse hippocampus. We found that microglia and astrocytes in COPD-NCDs mice were activated and neuronal and synaptophysin expression was decreased, indicating that chronic CS stimulation may induce hippocampal neuroinflammation, thereby causing neurocognitive impairment.

Previous studies have elucidated multiple pathways through which CS influences neurocognitive function. For instance, CS exposure has been shown to disrupt energy metabolism via the PPAR signaling pathway, exacerbating pathological changes and cognitive impairments in mice [50]. Beyond metabolic alterations, CS also perturbs critical neuronal signaling. Calcium, mainly in the form of calcium ions (Ca^{2+}), exists in neurons and plays an indispensable role in inducing and maintaining activity-dependent synaptic plasticity, which is the most closely related neurophysiological process to learning and memory [51]. This suggests that CS may impair cognitive ability by disrupting neuronal Ca^{2+} homeostasis [52]. Furthermore, a separate mechanistic study demonstrated that overexpressing sestrin2 attenuated hippocampal damage and neurocognitive disorders by rectifying CS-induced ferroptosis and synaptic protein alterations [7]. The timing of exposure is also critical, perinatal CS exposure (from pregnancy to 21 days postnatal) can induce aberrant hippocampal metabolism in adulthood, potentially constraining neurodevelopment and compromising learning and memory [53]. Compounding these effects, when CS exposure is combined with LPS, it synergistically triggers neuroinflammation in cognition-related brain regions and compromises BBB integrity [54]. Finally, 24-week CS exposure COPD model established by Dobric A et al. directly links these mechanisms to the disease context, confirming that neuropathological changes in the hippocampus underpin neurocognitive impairments in COPD [13]. Collectively, this evidence prompts a central question: what is the primary triggering mechanism of neuroinflammation in COPD-NCDs?

In COPD-NCDs patients, CS exposure causes pulmonary inflammation [55] which subsequently leads to the impairment of the pulmonary gas-blood barrier function [56], and airway wall remodeling is a significant feature of COPD [57]. Our pathological examination of the lung tissue of COPD mice also indicated that the structure of the gas-blood barrier had undergone significant changes. Thus, the inflammatory factors may further overflow into the bloodstream due to the destruction of the gas-blood barrier. Recent studies have shown that a fluid circulation axis may be established between the lungs and the brain [58, 59]. Inflammatory factors, metabolites and hormones can affect the structure and function of the brain through this fluid-based lung-brain axis. In particular, the "spill-over" of inflammation from the lungs into the bloodstream may damage brain neurons and lead to cognitive dysfunction. To explore whether this mechanism is involved in COPD-NCDs, we detected the levels of inflammatory factors IL-1β, IL-6 and TNF-α in the lung tissue, serum and brains of COPD-NCDs mice, and found that these indicators were significantly elevated in all three tissues of the COPD-NCDs group. This indicates the connectivity among the three.

To further explore the specific association mechanisms between COPD and NCDs, we performed 10-fold Genomics scRNA-seq on the whole brain cells of normal and COPD-NCDs mice. These cells were clustered according to gene expression, and these clusters were further organized into eight "meta-clusters" including astrocytes, endothelial cells, ependymal, fibroblasts, microglia, neurons, OPCs and oligodendrocytes. The proportions of endothelial cells and astrocytes were reduced in COPD-NCDs. Therefore, through further GO and KEGG analyses, we found that endothelial cells and astrocytes in COPD-NCDs were closely associated with disruption of endothelial cell tight junctions, synaptic dysfunction, and neurocognitive dysfunction disorders. This indicates that the permeability of the BBB may change in COPD-NCDs.

Homeostasis of the CNS is maintained by the BBB. The BBB is composed of capillary wall endothelial cells, pericytes, and astrocytes [60]. It is the interface between the CNS and the peripheral circulation, and plays a crucial role in regulating the transport of molecules into and out of the brain [61]. In this study, the mRNA levels and protein expression levels of Occludin, Claudin1 and ZO1 in the lungs and brains of COPD-NCDs mice were significantly lower than those of normal mice. EB staining shows increased lung and brain permeability in COPD-NCDs. Further IF detection also showed that the levels of CD31, Occludin, Claudin1 and ZO1 were significantly lower in COPD-NCDs compared to the NC group. This strongly indicates that the barrier function between the lungs and the brain of COPD-NCDs mice is impaired, inflammatory factors are more likely to transfer from the lungs to the brain, and the permeability of the blood-brain barrier is affected, thereby affecting the condition of COPD-NCDs.

Based on the above results, from a mechanistic perspective, we proposed that the disruption of the homeostasis of the CNS in COPD-NCDs mice consists of three-stage cascades: (1) Lung barrier disruption, leading to systemic inflammation; (2) BBB dysfunction, leading to neuroinflammation; (3) Neuronal and synaptic dysfunction, leading to cognitive dysfunction.

Direct visualization and dynamic monitoring of BBB integrity in COPD-NCDs represent a critical next step in validating the inflammation"spill-over"hypothesis. For instance, in vivo imaging techniques like MRI and PET enable non-invasive, real-time observation of BBB disruption and its correlation with neuroinflammation and behavioral outcomes [62]. MRI, strong in structural imaging, can also assess the severity of BBB leakage through specialized sequences (e.g., DCE-MRI) [63], potentially aiding in determining COPD-NCDs severity and progression. PET, centered on functional imaging,

can quantify BBB permeability to investigate alterations in molecular transport, thereby elucidating the effects of inflammatory mediators and metabolites on the barrier [64]. Clinically, integrated devices like"PET/MRI hybrid systems"are often employed to simultaneously capture structural details and molecular functional information, further enhancing diagnostic and research precision. Future in vivo imaging research may address several critical questions in COPD-NCDs: (1) Temporal progression: At which stage of CS exposure does BBB disruption occur? How does this correlate with elevated systemic inflammatory cytokine levels? (2) Spatial specificity: Is BBB disruption region-specific? We hypothesize a close association with the hippocampus, critical for learning and memory, while the prefrontal cortex may be particularly vulnerable. (3) Therapeutic monitoring: In vivo imaging can assess treatment efficacy following the administration of BBB-protective agents.

However, our research also has certain limitations. Firstly, in view of the experimental conditions, we are unable to apply magnetic resonance imaging (MRI) to observe the alterations in the permeability of the BBB more intuitively. Secondly, we cannot prove the direct correlation between the "spill- over" of inflammatory

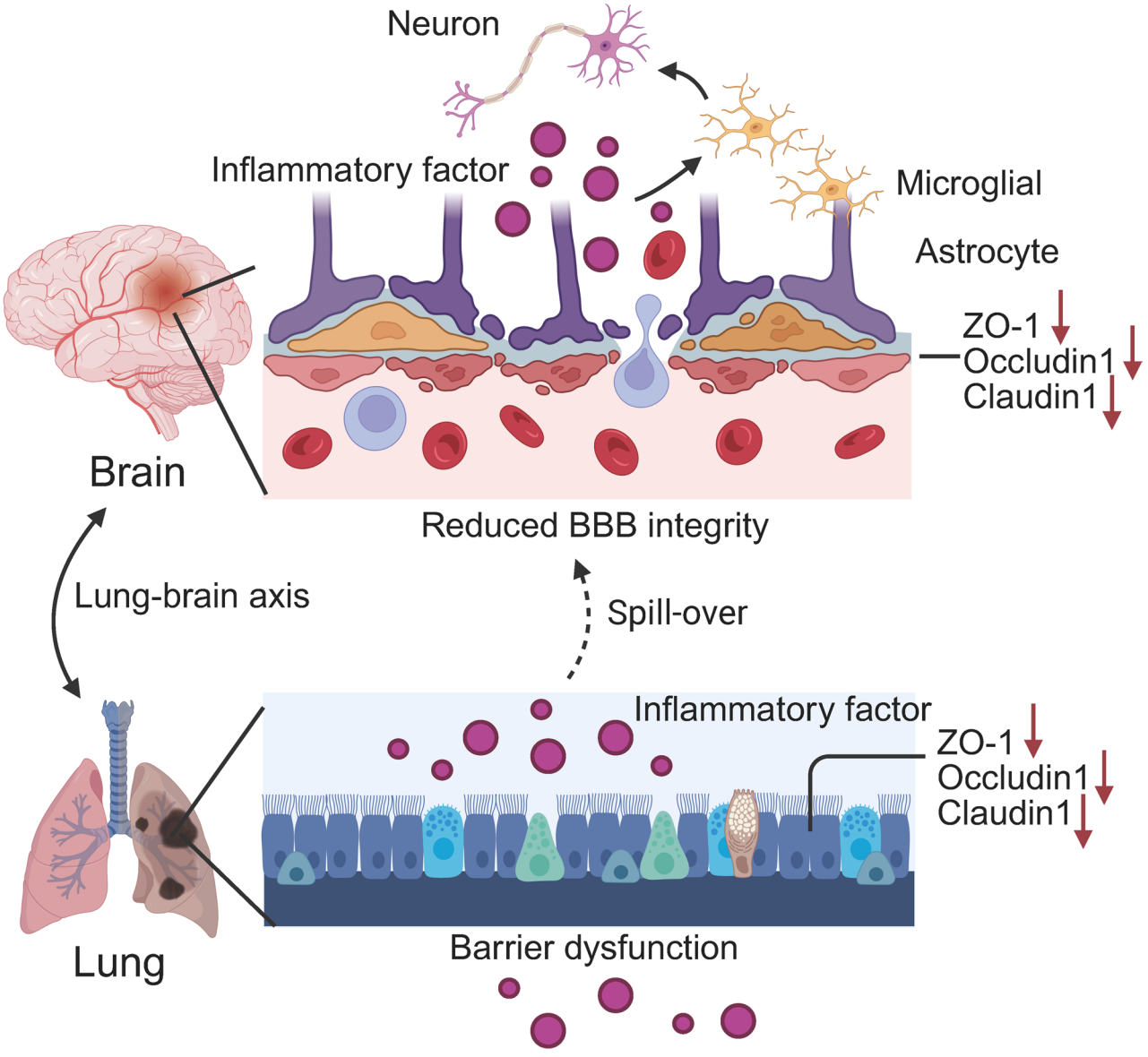

Fig. 10 Proposed mechanism of cigarette smoke-induced neurocognitive impairment via lung-brain barrier disruption. CS-induced lung barrier dysfunction permits inflammatory factor spill-over (IL-1β/IL-6/TNF-α) into circulation, compromising the BBB and triggering hippocampal neuroinflammation. There are three Key pathways involved in: (1) Structural disruption: Tight junction loss in lung and brain endothelial cells; (2) Functional spill-over: Inflammatory factors bypass compromised barriers; (3) Neuroglial activation: Microglia/astrocyte responses exacerbate neuronal damage

factors from the lungs to the brain, but can only indirectly prove that the neurocognitive impairment related to COPD is affected by the disruption of the barrier between the lungs and the brain, which leads to the "invasion" of inflammatory factors into the brain through the lung-brain axis. Although we observed concomitant lung-brain barrier disruption, direct causality requires future studies using conditional knockout models (e.g., endothelial-specific Claudin5 deletion). This mechanism deserves further exploration in the future, both as an innovative supplement to the mechanism of COPD-NCDs and as a new theoretical basis for the systemic symptoms of COPD.

Our research proposes a cascade model progressing from disruption of the air-blood barrier to BBB dysfunction and ultimately to cognitive impairment. Building upon this, future studies should further elucidate the intricate interactions along this axis. For instance, BBB integrity depends not only on endothelial tight junctions but also on the supportive role of the pericytes. Key areas for future research may include: (1) Establishing the timeline and causality of BBB disruption. (2) Decoding intercellular communication within the neurovascular units (involving endothelial cells, pericytes, astrocytes, and microglia), such as by mapping cell-type-specific gene expression profiles and interaction networks within these units in the context of COPD. Additionally, current therapeutic approaches for COPD-NCDs primarily explore anti-inflammatory and anti-oxidative stress mechanisms, such as corticosteroids and roflumilast. Therefore, the mechanism involving disruption of the air-blood barrier and BBB and the leakage of inflammatory mediators may offer new approaches and targets for improving the treatment of COPD-NCDs.

In conclusion, our study demonstrated a significant causal relationship between COPD and neurocognitive disorders. The longer the duration of COPD, the higher the risk of neurocognitive impairment. CS exposure induces a disruption of the lung barrier function, which in turn leads to the "spill-over" of inflammatory factors to the brain through the lung-brain axis, increasing the BBB permeability in the brain, thereby triggering neuroinflammation, damaging neuronal and synaptic function in the hippocampus and ultimately leading to neurocognitive impairment (Fig. 10). This study provides new insights into the possible mechanisms of COPD-NCDs, and may provide new ideas for potential treatments of COPD-NCDs.

Abbreviations

CS	Cigarette smoke
COPD	Chronic obstructive pulmonary disease
COPD-NCDs	COPD-related neurocognitive disorders
MR	Mendelian randomization
BBB	Blood-brain barrier
CNS	Central nervous system
OCLN	Occluding
ZO1	Zonula occludens 1
NRG1	Neuregulin1
ADAM	A disintegrin and metalloproteinase
ScRNA-seq	Single-cell RNA sequencing
WME	Weighted median
IVW	Inverse variance weighted
SM	Simple mode
WMO	Weighted mode
SPF	Specific pathogen free
WBP	Whole-body plethysmograph
Ti	Inspiratory time
Te	Expiratory time
PIF	Peak inspiratory flow
PEF	Peak expiratory flow
EF50	Expiratory flow at 50% tidal volume
MV	Minute ventilation
OF	Open field
NOR	Novel object recognition
MWM	Morris water maze
HE	Hematoxylin/eosin
ELISA	Enzyme-linked Immunosorbent assay
IF	Immunofluorescence
RT-qPCR	Real-time quantitative polymerase chain reaction
EB	Evans Blue
FEV0.1/FVC	Forced expiratory volume in 100ms/forced vital capacity
RI	Airway resistance
Cydn	Dynamic compliance
GO	Gene Ontology
KEGG	Kyoto Encyclopedia of Genes and Genomes
MRI	Magnetic resonance imaging

Supplementary Information

The online version contains supplementary material available at https://doi.org/10.1186/s12974-025-03629-7.

Supplementary Material 1.

Supplementary Material 2.

Authors' contributions

Conceptualization, F.W. and X.M.; writing—original draft preparation, X.Y.; computer graphics, X.Y.; writing—review and editing, H.X., S.B., Y.D., J.Z.; supervision, X.M. and Z.D.; project administration, X.M. and G.W.; funding acquisition, F.W. and X.M.

Funding

This study was supported by the Medical Basic Research Innovation Center of Airway Disease in North China, Key Laboratory of Pathobiology, Key Laboratory of Precision Infectious Diseases, Jilin Province (20200601011JC), Engineering Laboratory for Precision Prevention and Treatment of Common Diseases, Jilin Province (2022C036), Department of Science and Technology of Jilin Province: Key Scientific and Technological Research and Development Projects (20230204055YY), the Graduate Innovation Fund of Jilin University (Grant No. 2024CX129).

Data availability

Data available within the article or its supplementary materials.

Declarations

Ethics approval and consent to participate

All protocols involving animal experiments in this experiment were approved by the Ethics Committee for Animal Experiments of the College of Basic Medical Sciences of Jilin University (Approval No.2025–361), and were performed in accordance with the National Institutes of Health Guide for the Care and Use of Laboratory Animals.

Competing interests

The authors declare no competing interests.

Author details
[1]Department of Histology & Embryology, College of Basic Medical Sciences, Jilin University, Changchun 130021, China
[2]The Key Laboratory of Pathobiology, Ministry of Education, College of Basic Medical Sciences, Jilin University, Changchun 130021, China
[3]Department of Forensic Medicine, Basic Medical College, Jilin University, Changchun 130021, China
[4]College of Basic Medical Sciences, the Medical Basic Research Innovation Center of Airway Disease in North China, Key Laboratory of Pathobiology, Ministry of Education, Jilin University, Changchun 130021, China

Received: 21 July 2025 / Accepted: 10 November 2025
Published online: 30 December 2025

References

1. Lin J, Xia H, Yu J, Wang Y, Wang H, Xie D, Cheng C, Lu L, Bian T, Wu Y, Liu Q. circADAMTS6 via stabilizing CAMK2A is involved in smoking-induced emphysema through driving M2 macrophage polarization. Environ Int. 2024;190:108832.
2. Song X, Dou X, Chang J, Zeng X, Xu Q, Xu C. The role and mechanism of gut-lung axis mediated bidirectional communication in the occurrence and development of chronic obstructive pulmonary disease. Gut Microbes. 2024;16:2414805.
3. Celli BR, Anzueto A, Singh D, Hanania NA, Fabbri L, Martinez FJ, Soler X, Djandji M, Jacob-Nara JA, Rowe PJ, et al. The emerging role of Alarmin-Targeting biologics in the treatment of patients with COPD. Chest. 2025;167:1346–55.
4. De Luca SN, Vlahos R. Targeting accelerated pulmonary ageing to treat chronic obstructive pulmonary disease-induced neuropathological comorbidities. Br J Pharmacol. 2024;181:3–20.
5. Yang X, Guo AL, Pang YP, Cheng XJ, Xu T, Li XR, Liu J, Zhang YY, Liu Y. Astaxanthin attenuates environmental tobacco Smoke-Induced cognitive deficits: A critical role of p38 MAPK. Mar Drugs. 2019;17:24.
6. DiSabato DJ, Quan N, Godbout JP. Neuroinflammation: the devil is in the details. J Neurochem. 2016;139(Suppl 2):136–53.
7. Zhang DW, Yang MM, Zhou MX, Wei YY, Hu L, Hong M, Chen TT, Wang XM, Ding YC, Wei CS, et al. Sestrin2 alleviates cognitive impairment via inhibiting hippocampus ferroptosis in cigarette smoke-induced chronic obstructive pulmonary disease. Redox Biol. 2025;85:103673.
8. Alateeq R, Akhtar A, De Luca SN, Chan SMH, Vlahos R. Apocynin prevents cigarette Smoke-Induced Anxiety-Like behavior and preserves microglial profiles in male mice. Antioxid (Basel). 2024;13:855.
9. Wang J, Li X, Lei S, Zhang D, Zhang S, Zhang H, Li J. Risk of dementia or cognitive impairment in COPD patients: A meta-analysis of cohort studies. Front Aging Neurosci. 2022;14:962562.
10. Anstey KJ, von Sanden C, Salim A, O'Kearney R. Smoking as a risk factor for dementia and cognitive decline: a meta-analysis of prospective studies. Am J Epidemiol. 2007;166:367–78.
11. Tabaa ME, Mohammed El Tabaa M, Anis M, Mohamed Elgharabawy A, Borai El-Borai R. GLP-1 mediates the neuroprotective action of Crocin against cigarette smoking-induced cognitive disorders via suppressing HMGB1-RAGE/TLR4-NF-κB pathway. Int Immunopharmacol. 2022;110:108995.
12. De Luca SN, Brassington K, Chan SMH, Dobric A, Mou K, Seow HJ, Vlahos R. Ebselen prevents cigarette smoke-induced cognitive dysfunction in mice by preserving hippocampal synaptophysin expression. J Neuroinflammation. 2022;19:72.
13. Dobric A, De Luca SN, Seow HJ, Wang H, Brassington K, Chan SMH, Mou K, Erlich J, Liong S, Selemidis S, et al. Cigarette smoke exposure induces neurocognitive impairments and neuropathological changes in the hippocampus. Front Mol Neurosci. 2022;15:893083.
14. Singh B, Mielke MM, Parsaik AK, Cha RH, Roberts RO, Scanlon PD, Geda YE, Christianson TJ, Pankratz VS, Petersen RC. A prospective study of chronic obstructive pulmonary disease and the risk for mild cognitive impairment. JAMA Neurol. 2014;71:581–8.
15. Jia L, Liu X, Liu X, Guan Q, Tian Y, Li J, Zhao P. Bufei Yishen formula protects the airway epithelial barrier and ameliorates COPD by enhancing autophagy through the Sirt1/AMPK/Foxo3 signaling pathway. Chin Med. 2024;19:32.
16. Wei Y, Liu X, Jiang Y, Guan Q, Tian Y, Li J, Zhao P. Maintenance of airway epithelial barrier integrity via the Inhibition of AHR/EGFR activation ameliorates chronic obstructive pulmonary disease using effective-component combination. Phytomedicine. 2023;118:154980.
17. Tatsuta M, Kan OK, Ishii Y, Yamamoto N, Ogawa T, Fukuyama S, Ogawa A, Fujita A, Nakanishi Y, Matsumoto K. Effects of cigarette smoke on barrier function and tight junction proteins in the bronchial epithelium: protective role of Cathelicidin LL-37. Respir Res. 2019;20:251.
18. Krüger K, Seimetz M, Ringseis R, Wilhelm J, Pichl A, Couturier A, Eder K, Weissmann N, Mooren FC. Exercise training reverses inflammation and muscle wasting after tobacco smoke exposure. Am J Physiol Regul Integr Comp Physiol. 2018;314:R366–76.
19. He Q, Li P, Han L, Yang C, Jiang M, Wang Y, Han X, Cao Y, Liu X, Wu W. Revisiting airway epithelial dysfunction and mechanisms in chronic obstructive pulmonary disease: the role of mitochondrial damage. Am J Physiol Lung Cell Mol Physiol. 2024;326:L754–69.
20. Aghapour M, Raee P, Moghaddam SJ, Hiemstra PS, Heijink IH. Airway epithelial barrier dysfunction in chronic obstructive pulmonary disease: role of cigarette smoke exposure. Am J Respir Cell Mol Biol. 2018;58:157–69.
21. Finigan JH, Faress JA, Wilkinson E, Mishra RS, Nethery DE, Wyler D, Shatat M, Ware LB, Matthay MA, Mason R, et al. Neuregulin-1-human epidermal receptor-2 signaling is a central regulator of pulmonary epithelial permeability and acute lung injury. J Biol Chem. 2011;286:10660–70.
22. Mishra R, Foster D, Vasu VT, Thaikoottathil JV, Kosmider B, Chu HW, Bowler RP, Finigan JH. Cigarette smoke induces human epidermal receptor 2-Dependent changes in epithelial permeability. Am J Respir Cell Mol Biol. 2016;54:853–64.
23. Bajinka O, Simbilyabo L, Tan Y, Jabang J, Saleem SA. Lung-brain axis. Crit Rev Microbiol. 2022;48:257–69.
24. De Luca SN, Chan SMH, Dobric A, Wang H, Seow HJ, Brassington K, Mou K, Alateeq R, Akhtar A, Bozinovski S, Vlahos R. Cigarette smoke-induced pulmonary impairment is associated with social recognition memory impairments and alterations in microglial profiles within the Suprachiasmatic nucleus of the hypothalamus. Brain Behav Immun. 2023;109:292–307.
25. Ewees MG, El-Mahdy MA, Hannawi Y, Zweier JL. Tobacco cigarette smoking induces cerebrovascular dysfunction followed by oxidative neuronal injury with the onset of cognitive impairment. J Cereb Blood Flow Metab. 2025;45:48–65.
26. Kadry H, Noorani B, Bickel U, Abbruscato TJ, Cucullo L. Comparative assessment of in vitro BBB tight junction integrity following exposure to cigarette smoke and e-cigarette vapor: a quantitative evaluation of the protective effects of Metformin using small-molecular-weight paracellular markers. Fluids Barriers CNS. 2021;18:28.
27. Huang X, Hussain B, Chang J. Peripheral inflammation and blood-brain barrier disruption: effects and mechanisms. CNS Neurosci Ther. 2021;27:36–47.
28. Pelgrim CE, van Ark I, van Berkum RE, Schuitemaker-Borneman AM, Flier I, Leusink-Muis T, Janbazacyabar H, Diks MAP, Gosker HR, Kelders M, et al. Effects of a nutritional intervention on impaired behavior and cognitive function in an emphysematous murine model of COPD with endotoxin-induced lung inflammation. Front Nutr. 2022;9:1010989.
29. Skrivankova VW, Richmond RC, Woolf BAR, Davies NM, Swanson SA, VanderWeele TJ, Timpson NJ, Higgins JPT, Dimou N, Langenberg C, et al. Strengthening the reporting of observational studies in epidemiology using Mendelian randomisation (STROBE-MR): explanation and elaboration. BMJ. 2021;375:n2233.
30. Guan X, Yuan Y, Wang G, Zheng R, Zhang J, Dong B, Ran N, Hsu AC, Wang C, Wang F. Ginsenoside Rg3 ameliorates acute exacerbation of COPD by suppressing neutrophil migration. Int Immunopharmacol. 2020;83:106449.
31. Hu D, Mo X, Luo J, Wang F, Huang C, Xie H, Jin L. 17-DMAG ameliorates neuroinflammation and BBB disruption via SOX5 mediated PI3K/Akt pathway after intracerebral hemorrhage in rats. Int Immunopharmacol. 2023;123:110698.
32. Hosseini A, Sheibani M, Valipour M. Exploring the therapeutic potential of BBB-Penetrating phytochemicals with p38 MAPK modulatory activity in addressing oxidative Stress-Induced neurodegenerative Disorders, with a focus on alzheimer's disease. Phytother Res. 2024;38:5598–625.
33. Kahnert K, Jörres RA, Behr J, Welte T. The diagnosis and treatment of COPD and its comorbidities. Dtsch Arztebl Int. 2023;120:434–44.
34. Guo P, Li R, Piao TH, Wang CL, Wu XL, Cai HY. Pathological mechanism and targeted drugs of COPD. Int J Chron Obstruct Pulmon Dis. 2022;17:1565–75.
35. Yu X, Xiao H, Liu Y, Dong Z, Meng X, Wang F. The Lung-Brain axis in chronic obstructive pulmonary Disease-Associated neurocognitive dysfunction: mechanistic insights and potential therapeutic options. Int J Biol Sci. 2025;21:3461–77.

36. Wang C, Yu X, Yu X, Xiao H, Song Y, Wang X, Zheng H, Chen K, An Y, Zhou Z, et al. Gut flora-derived succinate exacerbates allergic airway inflammation by promoting protein succinylation. Redox Biol. 2025;82:103623.
37. Shu MJ, Li JR, Zhu YC, Shen H. Migraine and ischemic stroke: A Mendelian randomization study. Neurol Ther. 2022;11:237–46.
38. Burgess S, Thompson SG. Interpreting findings from Mendelian randomization using the MR-Egger method. Eur J Epidemiol. 2017;32:377–89.
39. Bowden J, Davey Smith G, Haycock PC, Burgess S. Consistent Estimation in Mendelian randomization with some invalid instruments using a weighted median estimator. Genet Epidemiol. 2016;40:304–14.
40. Upadhyay P, Wu CW, Pham A, Zeki AA, Royer CM, Kodavanti UP, Takeuchi M, Bayram H, Pinkerton KE. Animal models and mechanisms of tobacco smoke-induced chronic obstructive pulmonary disease (COPD). J Toxicol Environ Health B Crit Rev. 2023;26:275–305.
41. Wright JL, Cosio M, Churg A. Animal models of chronic obstructive pulmonary disease. Am J Physiol Lung Cell Mol Physiol. 2008;295:L1–15.
42. Zeng Z, Li T, Liu X, Ma Y, Luo L, Wang Z, Zhao Z, Li H, He X, Zeng H, et al. DNA dioxygenases TET2 deficiency promotes cigarette smoke induced chronic obstructive pulmonary disease by inducing ferroptosis of lung epithelial cell. Redox Biol. 2023;67:102916.
43. Wang Z, Deng M, Xu W, Li C, Zheng Z, Li J, Liao L, Zhang Q, Bian Y, Li R, et al. DKK3 as a diagnostic marker and potential therapeutic target for sarcopenia in chronic obstructive pulmonary disease. Redox Biol. 2024;78:103434.
44. Zhou JS, Li ZY, Xu XC, Zhao Y, Wang Y, Chen HP, Zhang M, Wu YF, Lai TW, Di CH, et al. Cigarette smoke-initiated autoimmunity facilitates sensitisation to elastin-induced COPD-like pathologies in mice. Eur Respir J. 2020;56:2000404.
45. Lv Z, Hu P, Jiang Y, Yang W, Wang R, Wang K, Fan X. Changes in Spatial Working Memory in Stable Chronic Obstructive Pulmonary Disease: A Retrospective Study. Biomed Res Int. 2020;2020:7363712.
46. Nadar MS, Hasan AM, Alsaleh M. The negative impact of chronic tobacco smoking on adult neuropsychological function: a cross-sectional study. BMC Public Health. 2021;21:1278.
47. Paul RH, Brickman AM, Cohen RA, Williams LM, Niaura R, Pogun S, Clark CR, Gunstad J, Gordon E. Cognitive status of young and older cigarette smokers: data from the international brain database. J Clin Neurosci. 2006;13:457–65.
48. Brunette AM, Warner K, Holm KE, Meschede K, Wamboldt FS, Kozora E, Moser DJ, Make BJ, Crapo JD, Moreau KL, et al. Daily activities: the impact of COPD and cognitive dysfunction. Arch Clin Neuropsychol. 2021;36:acaa090. 767 779 – 767.
49. Deng X, Fu J, Song Y, Xu B, Ji Z, Guo Q, Ma S. Glucocorticoid receptor dysfunction orchestrates inflammasome effects on chronic obstructive pulmonary disease-induced depression: A potential mechanism underlying the cross talk between lung and brain. Brain Behav Immun. 2019;79:195–206.
50. Xie Y, Wang H, Zhang Y, Lin B, Chen Y, Li K, Tang H, Sun Q. Cigarette smoke-induced PPAR signaling dysregulation accelerates alzheimer's disease pathogenesis and cognitive decline in 5xFAD mice. Food Chem Toxicol. 2025;203:115596.
51. Kumar A. Calcium signaling during brain aging and its influence on the hippocampal synaptic plasticity. Adv Exp Med Biol. 2020;1131:985–1012.
52. Zhang H, Zhou H, Guo X, Zhang G, Xiao M, Wu S, Jin C, Yang J, Lu X. Cigarette smoke triggers calcium overload in mouse hippocampal neurons via the ΔFOSB-CACNA2D1 axis to impair cognitive performance. Ecotoxicol Environ Saf. 2023;258:114996.
53. Neal RE, Jagadapillai R, Chen J, Webb C, Stocke K, Greene RM, Pisano MM. Developmental cigarette smoke exposure II: hippocampus proteome and metabolome profiles in adult offspring. Reprod Toxicol. 2016;65:436–47.
54. Pelgrim CE, Wang L, Peralta Marzal LN, Korver S, van Ark I, Leusink-Muis T, Braber S, Folkerts G, Garssen J, van Helvoort A, Kraneveld AD. Increased exploration and hyperlocomotion in a cigarette smoke and LPS-induced murine model of COPD: linking pulmonary and systemic inflammation with the brain. Am J Physiol Lung Cell Mol Physiol. 2022;323:L251–65.
55. Cheng M, Yan X, Wu Y, Zeng Z, Zhang Y, Wen F, Chen J, Wang T. Qingke Pingchuan granules alleviate airway inflammation in COPD exacerbation by inhibiting neutrophil extracellular traps in mice. Phytomedicine. 2025;136:156283.
56. Nwozor KO, Hackett TL, Chen Q, Yang CX, Aguilar Lozano SP, Zheng X, Al-Fouadi M, Kole TM, Faiz A, Mahbub RM, et al. Effect of age, COPD severity, and cigarette smoke exposure on bronchial epithelial barrier function. Am J Physiol Lung Cell Mol Physiol. 2025;328:L724–37.
57. Zhou H, Lai Y, Zhu Y, Shao F, Ma G, Yang N, Ma X, Sun Y, Shi Q. Quercetin improves airway remodeling in COPD rats by suppressing phenotypic switch of ASMCs via inhibiting the Wnt5a/β-catenin pathway. Phytomedicine. 2025;139:156491.
58. Hu J, Guo J, Wu C, He X, Jing J, Tao M. Annexin A5 derived from lung alleviates brain damage after ischemic stroke. Brain Res. 2025;1846:149303.
59. He J, Zhang Y, Guo Y, Guo J, Chen X, Xu S, Xu X, Wu C, Liu C, Chen J, et al. Blood-derived factors to brain communication in brain diseases. Sci Bull (Beijing). 2024;69:3618–32.
60. Sun Y, Koyama Y, Shimada S. Inflammation from peripheral organs to the brain: how does systemic inflammation cause neuroinflammation? Front Aging Neurosci. 2022;14:903455.
61. Takata F, Tominaga K, Koga M, Dohgu S, Futagami K, Yamauchi A, Kataoka Y. Elevated permeability of the blood-brain barrier in mice intratracheally administered Porcine pancreatic elastase. J Pharmacol Sci. 2015;129:78–81.
62. Karlsson L, Vogel J, Arvidsson I, Åström K, Strandberg O, Seidlitz J, Bethlehem RAI, Stomrud E, Ossenkoppele R, Ashton NJ, et al. Machine learning prediction of tau-PET in alzheimer's disease using plasma, MRI, and clinical data. Alzheimers Dement. 2025;21:e14600.
63. Sasannia S, Leigh R, Bastani PB, Shin HG, van Zijl P, Knutsson L, Nyquist P. Blood-brain barrier breakdown in brain ischemia: insights from MRI perfusion imaging. Neurotherapeutics. 2025;22:e00516.
64. Chung KJ, Abdelhafez YG, Spencer BA, Jones T, Tran Q, Nardo L, Chen MS Jr., Sarkar S, Medici V, Lyo V, et al. Quantitative PET imaging and modeling of molecular blood-brain barrier permeability. Nat Commun. 2025;16:3076.

Publisher's note